To the Graduate Council:

I am submitting herewith a thesis written by Kathleen Patricia Baker entitled "Application of Double Beam Sodium Line Reversal to Determine Absolute Temperature". I have examined the final copy of this thesis for form and content and recommend that it be accepted in partial fulfillment of the requirements for the degree of Master of Science, with a major in Physics.

Arthur A. Mason, Major Professor

We have read this thesis and
recommend its acceptance:

Accepted for the Council:

Associate Vice Chancellor
and Dean of The Graduate School

Application of Double Beam Sodium Line Reversal to Determine Absolute Temperature

A Thesis

Presented for the

Master of Science

Degree

The University of Tennessee, Knoxville

Kathleen Patricia Baker

August, 1995

Acknowledgments

I would like to thank those who have assisted me during the course of this thesis. I thank Linwood L. Price, Michael S. Smith, and Bill J. McClure for their constant patience, support, and assistance during this work. Their friendship and encouragement have been greatly appreciated. Also, I extend thanks to those who served on the thesis committee: Dr. Arthur A. Mason, major professor; Dr. Horace Crater; and Dr. Christian Parigger. Thanks must also go to the Arnold Engineering Development Center and Micro Craft Technology for providing the laboratories and operating personnel necessary for completion of this thesis.

I wish to extend special thanks to my parents for teaching me two important lessons: do not fear difficulties, persevere through them; and do not dream about goals, achieve them.

Abstract

Equilibrium or near-equilibrium absolute temperatures are measured by the use of the line reversal method, which involves the comparison of broad-band, continuum radiation with narrow molecular or atomic signatures of selected seed species. The temperature is obtained by the adjustment of the continuum radiation intensity to or near the reversal of seed absorption and seed emission. The technique of sodium line reversal is addressed in a laboratory setting in support of application to the Arnold Engineering Development Center (AEDC) Impulse Facility.

Development of the double beam method included initial, static measurements in a flat flame burner, and time resolved measurements in a laboratory shock tube. Final measurements in the Impulse Facility were not possible due to monetary constraints; however, necessary calculations and investigations were performed as if the tests were to occur. Arguments for performing these measurements are presented.

General theory of the sodium line reversal technique is presented and referenced. It includes a discussion of the Planck's blackbody radiation distribution and its relationship to true temperature through the emissivity of a material that is not a blackbody. The atomic theory of the sodium D lines at 589.0nm and 589.6nm is briefly reviewed.

Instrumentation for data collection is discussed in detail. This includes optical and electronic equipment. Where appropriate, photographs are included for clarification of optical arrangements. Problems occurring along the way are presented and dealt with, for example, temperature errors due to optical alignment, and methods of introducing salt into the different test environments.

At each stage of development of the application for the burner and the shock tube, experimental results are compared to expected results. The expected results are generated by computer calculations and by thermocouple measurements of the flame. Good agreement is found for both the flame and the shock tube. Uncertainty calculations, such

as calibration uncertainty and signal to noise ratios, accompany the results for both the flame and the shock tube.

Table of Contents

Chapter — Page

I. Introduction 1

II. Theory of Sodium line reversal 3

A. Planck's radiation law 3

B. Sodium: atomic theory 5

C. Line reversal: double beam method 7

III. General experimental method 9

A. Instrumentation 9

B. Data collection and reduction methods 11

IV. Uncertainty analysis 13

A. Uncertainty corrections 13

B. Optical and electronic systems 15

C. Final uncertainty values 17

V. Application of method to flat-flame burner 18

A. Description of burner 18

B. Optical arrangement 18

C. Introduction of sodium to the flame 20

D. Determination of expected temperature 21

E. Experimental results and comparison to calculated results 22

VI. Application of method to shock tube 28

A. Description of shock tube 28

B. Optical arrangement 29

C. Introduction of sodium to the shock tube 30

D. Additional instrumentation for timing and triggering 32

E. Determination of expected results 33

F. Experimental results and comparison to calculated results 36

VII. Theoretical application to Impulse Facility 42

A. Description of Impulse Facility 42

B. Optical arrangement 43

C. Introduction of sodium 44

D. Triggering, timing 45

E. Additional considerations 45

1. Doppler shifting 45

2. Boundary layer 46

F. Expected results 47

VIII. Conclusions and suggestions for future research 49

References 51

Appendices 55

A. SODREV3.FOR 56

B. SODREV4.FOR 59

Vita 62

List of Figures

Figure		Page
1.1.	Temperature Ranges for the Various Laboratories and Facilities and Temperature Range for the Sodium Line Reversal Experiment	2
2.1.	Sodium D-Line Transitions	7
3.1.	Spectral Radiance versus Input Current	9
3.2.	Brightness Temperature versus Input Current	10
4.1.	Initial Filament Orientation	13
4.2.	Initial Filament Orientation with Gas Image	14
4.3.	Final Filament Orientation	15
5.1.	Experimental Set-up for Flat Flame Burner	18
5.2.	Typical Flame Trace and Calculation Output	23
5.3.	Independence of Temperature on Sodium Amount	24
5.4.	Temperature versus Methane Content	26
5.5.	Comparison of Calculated and Measured Temperatures	27
6.1.	Shock Tube Diagram	28
6.2.	Experimental Set-up for Shock Tube	29
6.3.	Calculated Shock Tube Temperature	34
6.4.	Helium Arrival in Shock Tube	35
6.5.	Shock Tube Temperature Measurement using Salt-Methanol Solution	37
6.6.	Shock Tube Temperature Measurement using Solid Salt	39
6.7.	Comparison of Calculated and Measured Temperatures	40
7.1.	Diagram of Impulse Facility	42
7.2.	Experimental Set-up for Impulse Facility	44

List of Tables

Table		Page
4.1.	Optical Uncertainty Values	16
4.2.	Temperature Uncertainty Values	17

I. Introduction

Temperature is a fundamental parameter in the study and calibration of aerospace test facilities. Temperature, along with density, pressure, Mach number, and molecular and atomic constituents of the test gas are all necessary to characterize the flow in a facility.

Although temperature measurements can be achieved using probes that sample a portion of the gas in the flow, non-intrusive measurement techniques are more desirable and, indeed, superior. Intrusive techniques, such as probes, disrupt the flow about the test bodies, thereby changing that which they are intended to measure. Sodium line reversal (SLR), being an optical technique, is non-intrusive, and is therefore a preferred method.

SLR has been applied to many systems of heated gases. It has been applied numerous times to flames and has been shown to be a reliable method for temperature determination in flames [1]. In fact, in its more recent applications, it has been used as the standard for comparison of temperature to other experimental methods of determination [2]. Line reversal has also been applied with good results to coal fired MHD plasmas [3, 4]. SLR has been used on shock heated gases as both a single and double beam method in shock tubes as well [5, 6]. In both of the latter two examples, line reversal was used to gather time-resolved temperature measurements during flow time.

The application of SLR to the Impulse Facility at AEDC would serve two purposes. The first purpose, the obvious one, would be the determination of gas temperature during the flow. The second purpose would be a measurement of the useful test time, a by-product of the temperature measurement. The facility test-time duration is governed by the arrival of the cool, helium driver gas (explained in Chapter VII). When this arrives, the temperature drops very quickly. Therefore, this temperature drop could be used to give a measure of the test time duration, which is another necessary parameter in calibration of a transient flow facility.

Although the line reversal technique has been widely used, its application to each new apparatus introduces problems in the experimental realization. The Impulse Facility, a relatively expensive facility to run, could not be used to work out all of the problems of this particular line reversal set-up. Problems were approached and solved in the least difficult and least expensive setting possible. Optical errors were corrected while working with the flat flame burner. Decisions about timing and triggers were made during work on the shock tube. Had this not been the method of approach, these problems would have been worked out at the Impulse Facility in a more difficult, more costly environment. Clearly, that would have been less desirable.

The range of temperatures covered by the SLR system and the three members of the experimental progression make this method a good choice. Figure 1.1 shows the temperature ranges of the experiment and the temperature ranges for all of the different applications. It shows that the SLR method will be suitable for all of the suggested laboratories and facilities for at least some of the test conditions that can be achieved.

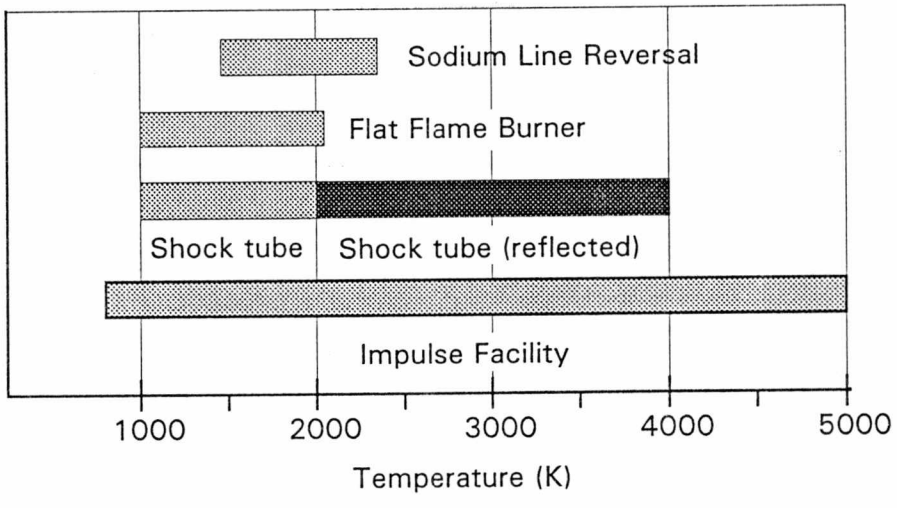


Figure 1.1. Temperature Ranges for the Various Laboratories and Facilities and Temperature Range for the Sodium Line Reversal Experiment

II. Theory of Sodium line reversal

A. Planck's radiation law

The theory of line reversal is based on the Planck blackbody equation, Eq. 1 [7], where L_B is the spectral radiance (Watts/mm^2/nm/steradians), h is Planck's constant, c is the speed of light, λ is the wavelength, T is the temperature, and k is Boltzmann's constant:

$$L_B(\lambda,T)=\frac{2hc^2}{\lambda^5}\frac{1}{e^{hc/\lambda kT_B}-1}. \qquad (1)$$

In a system under local thermodynamic equilibrium (LTE), the population ratio of states can be described by the Maxwell-Boltzmann relationship or distribution [7],

$$\frac{N_2}{N_1}=\frac{g_2}{g_1}e^{-(E_2-E_1)/kT}, \qquad (2)$$

where N_i is the population, g_i is the statistical weight, or degeneracy, and E_i is the energy state of the i^{th} level. This can be derived from the principle of detailed balance in which, under equilibrium, the collision and radiation rates must balance separately [7]. Because of the dependence on the Maxwell-Boltzmann distribution, the relative population of the energy levels depends mostly on temperature. The temperature (T) in Eq. 2 is a measure of the electronic excitation temperature for the particular transition [1].

Line reversal is a method for comparing the populations of the upper and lower states under equilibrium, thereby obtaining a temperature. When a spectral line of an absorbing/emitting medium is viewed against a background source, it will appear as a line against the continuous spectra of the source. With a source of varying intensity, the line will appear dark against the background when the source radiation at that wavelength is

more intense than the gas, and will appear bright against the background when it is less intense. The point where the line disappears, where they reverse their intensity with respect to the background, is called the reversal point [3, 7]. Kirchhoff's Law states that, at equilibrium, the absorptivity of a gas is equal to its emissivity. Using this and the fact that there exists a Boltzmann distribution of population, it can be shown that the source function, the ratio of the emission and absorption coefficients of the source gas, reduces to the Planck blackbody distribution, Eq. 1 [8]. Therefore, at the reversal point, the temperature of the source equals that of the gas for the given transition [7].

However, if the source used is not a blackbody, as in the case of the tungsten lamp used, then some alterations must be made to Eq. 1. For (λT_B) small compared to $^{hc}/_{k}$, which is the case for the sodium D lines at about 2000 K, the spectral radiance in Eq. 1 can be approximated by the use of Wien's approximation

$$L_W \cong \frac{2hc^2}{\lambda^5} e^{-hc/\lambda k T_B}. \qquad (3)$$

After algebraic manipulation, this gives a brightness temperature, T_B,

$$T_B = [\frac{\lambda k}{hc} \ln(\frac{2hc^2}{L_W \lambda^5})]^{-1}. \qquad (4)$$

This is the blackbody temperature, the temperature at which a blackbody would be at the same spectral radiance, L_W [7]. The actual, or true temperature of the source (T_t) is given by [7]

$$L_W(\lambda, T_B) = \varepsilon(\lambda, T_t) L_W(\lambda, T_t), \qquad (5)$$

where ε is the emissivity of the source material as a function of wavelength and temperature. Emissivity values depend on the material of the source and on the condition of that material. Therefore, tabulated values in which the condition of the experimental material matched that of the lamp used were chosen [9, 10]. Eqs. 3 and 5 then give the true temperature of the material, T_t, as a function of the brightness temperature, wavelength, and emissivity as the solution of the transcendental equation

$$T_t = \{ 1/T_B + \frac{\lambda k}{hc} \ln[\varepsilon(\lambda, T_t)] \}^{-1}. \qquad (6)$$

This true temperature of the source, with emissivity taken into account is the temperature that matches the gas temperature at the reversal point.

B. Sodium: atomic theory

There have been several different molecules and transitional lines used for line reversal. These include potassium (766.5, 769.9nm) [3, 4]; chromium (425.4, 427.4, 428.9nm) [11]; indium (451.1nm) [6]; the OH radical in the ultraviolet (306.4nm) [2]; CO_2 in the far infrared (4.4μm); and of course, the sodium D lines (D_2, 589.0nm; D_1, 589.6nm) [5, 6, 12, 13]. All that is necessary of the spectral line is that it be a strong transition, as are the sodium D lines. By far, the most popular of these is sodium. It is centered in the visible spectrum where special ultraviolet or infrared detectors are not needed. Also, in the form of NaCl, table salt, it is safe and easy to handle and inexpensive to purchase. The dissociation of the sodium and the chloride happens very quickly, on the order of a few microseconds [5]. If it did not, there would be a lag time before emission and absorption could begin.

The excitation of the sodium atoms is caused by collisions between sodium atoms and molecules, usually N_2, in the experimental gas. Internal vibrational energy of the

molecules is converted into electronic energy of the atoms by these inelastic collisions [1, 14].

The electron configuration of sodium is [15]

$$1s^2\,2s^2\,2p^6\,3s \qquad (7)$$

where the final electron, 3s, is the one that undergoes transitions. The quantum numbers of the last term are n=3, l=0, m_l=0, and s=1/2 [$(3, 0, 0, 1/2)_{nlms}$], where n represents the energy level, l is the orbital angular momentum (0 representing the 's' subshell), m is the z-component of the orbital angular momentum, and s is the spin. Using a total angular momentum quantum number, j=l+s, the quantum numbers can be taken as n=3, l=0, j=+/- 1/2, and m_j=0 [$(3, 0, +/- 1/2, 0)_{nljm}$)]. The two levels given for j are from the fact that the one electron in the m shell can have either spin up (+1/2) or spin down (-1/2).

When the outside electron is excited, it jumps to a higher subshell, 3p. The quantum numbers change to [$(3, 1, 3/2 \text{ or } 1/2, m_j)_{nljm}$]. This gives rise to a fine splitting of the spectra. The splitting of the spectra into two transitions can be represented by [15]

$$^2P_{1/2} \quad \text{and} \quad ^2P_{3/2}, \qquad (8)$$

where the superscript '2' represents the two-fold degeneracy, given by 2S+1, P represents the transition from the p subshell, and the subscripts are the j quantum numbers [7]. The m_j quantum number gives rise to the further degeneracy of these two transitions. In the experiment, due to spectral resolution constraints, the splitting caused by this degeneracy can be ignored. However, m_j also gives a relative intensity of the transitions. The degeneracy is given by 2j+1 [7]. Therefore, there is a degeneracy of 2 and 4, respectively for the levels in Eq. 8. Thus, the $P_{3/2}$ level is the stronger of the two. This transition at

589.0nm (the weaker one being at 589.6nm) is the one used for the line reversal measurements. The transitions and splittings are represented pictorially in Fig. 2.1.

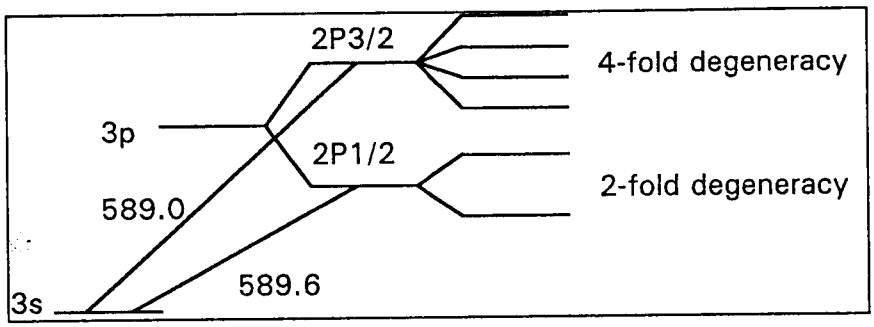


Figure 2.1. Sodium D-Line Transitions

C. Line reversal: double beam method

In basic line reversal measurements, the intensity of the background source is varied until the reversal point is reached. In shock tube work the lamp intensity is held constant and a difference between the level of emission or absorption is used to find how low or high the temperature of the source is with respect to the temperature of the test gas. The apparent strengths of the emission or absorption are a function of how much sodium is in the path of viewing. If this amount is not constant, as is probably the case in a shock tube, then this fluctuation must be calculated out as an uncertainty. However, if two different intensities of light are used as a background continuum, corresponding to temperatures one higher and one lower than the temperature of the test gas, then two measurements can be made, one absorption and one emission. The two intensities are chosen prior to the test by considering the initial conditions of the flame or shock tube, which allow an estimate of the temperature to be made. A beamsplitter is placed at the source to form the two backgrounds. The equations for the true temperatures of these two beams are given by Eqs. 9 and 10.

$$T_1 = \{ 1/T_t - \frac{\lambda k}{hc} \ln[\tau \tau_{bs} \tau_l \tau_w] \}^{-1} \qquad (9)$$

$$T_2 = \{ 1/T_t - \frac{\lambda k}{hc} \ln[\tau \rho_{bs} \rho_{m1} \rho_{m2} \tau_l \tau_w] \}^{-1} \qquad (10)$$

They are both given in terms of the true temperature of the full source. The ρ, τ represent reflection and transmission coefficients of optics in the beam path, such as Mirror1, Lens, Window, and BeamSplitter. T_1, in Eq. 9, is the higher temperature. By using two beams of slightly different temperature, there is no need to account for fluctuations in the amount of sodium. The temperature can be calculated using an interpolation between the signal from emission and the signal from absorption [6]. The temperature of the gas, T_{gas} is then given by

$$T_{gas} = T_2 + \frac{e(T_1 + T_2)}{a + e}, \qquad (11)$$

where 'a' and 'e' represent the absorption and emission signal, respectively.

III. General experimental method

A. Instrumentation

The background source used for the line reversal measurements was a General Electric Company Type GE 30A/T24/17 tungsten ribbon lamp. It was powered by an Electronic Instruments Inc. TCR power supply. This source was designed to operate at an input current of 30A, however, to gain more flexibility in temperature measurements, the lamp was calibrated by the Precision Measurement Equipment Laboratory (PMEL), AEDC for spectral radiance versus input current. The calibration result is shown in Fig. 3.1.

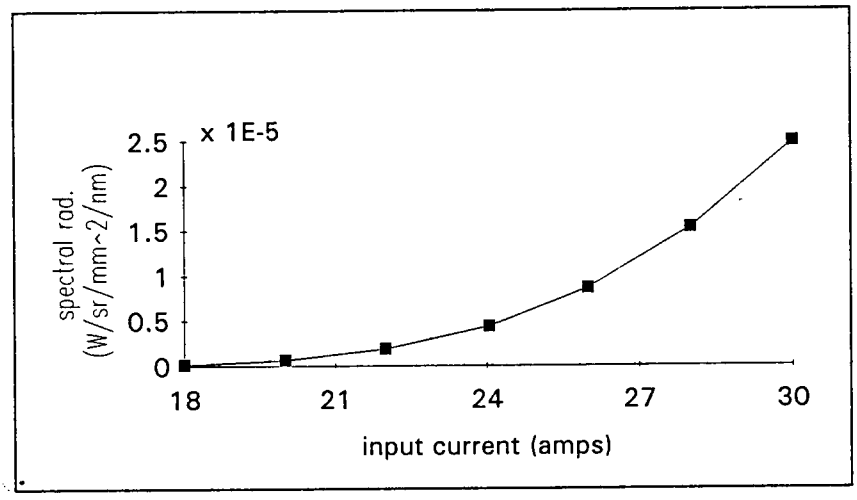


Figure 3.1. Spectral Radiance versus Input Current

The calibration allows the spectral radiance of the source to be set using the input current control, which, on this power supply, appears as a potentiometer. When the blackbody theory is applied in the Wien approximation, Eq. 3, the dependence of temperature versus input current can be obtained. This is shown in Fig. 3.2.

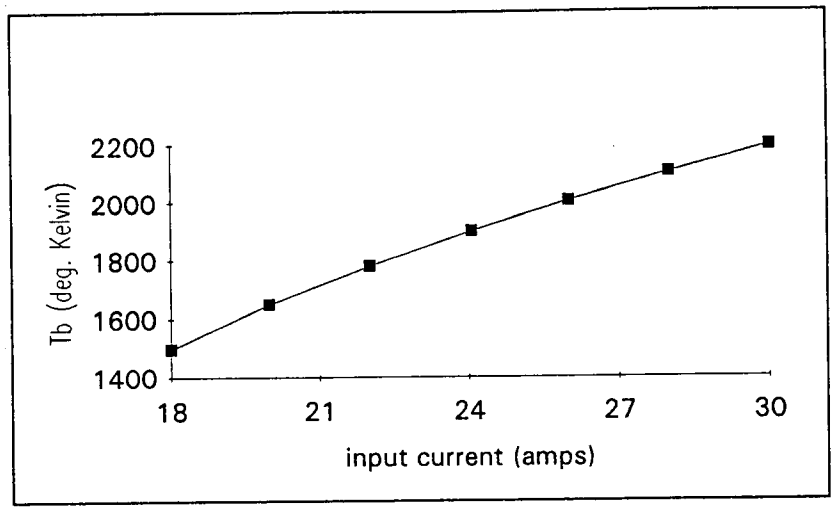


Figure 3.2. Brightness Temperature versus Input Current

Consequently, the blackbody temperature for the spectral radiance of the source can be set as a function of the input current. This can be used, along with the equations of chapter II, to find the true temperature as a function of current.

Transmission and reflection factors for the optics that were used in the light path for directing the light were taken from the factory specifications for their make-up material. They will be dealt with further in the chapter on uncertainty analysis.

The beamsplitter used for forming the two light sources was coated and calibrated at PMEL, AEDC.

Two spectrometers were needed for the measurement. (Two matched filters, centered at the sodium line could have been used, but were not available.) An Acton f/3.8, 0.275m spectrometer with a 1200g/mm, holographic grating, and a GCA/MacPherson f/6, 0.3m spectrometer with a 1200g/mm grating blazed at 150nm were used. A slit width of 200μm was set on each spectrometer. This slit width was chosen during work on the flame for optimum signal conditions. For the MacPherson, a visible light wavelength calibration was necessary. This was done during work on the flame, and the strong sodium line was found to be at 588.05nm on the wavelength dial. For the

Acton, no calibration was necessary, however, the wavelength was checked, again during work on the flame, and the sodium line was found to be at 588.9nm on the spectrometer setting. Problems occurring because of the differences between the two spectrometers are dealt with in Chap. 5, Sec. B.

The collection of data also required electronic equipment. There were three digital oscilloscopes used for different situations: Nicolet 430E 10MHz, 2-channel; Lecroy 9310, 300MHz, 2-channel; Lecroy 9314A, 400MHz, 4-channel. Two Burle C31034A photomultiplier tubes (PMTs) were used. They were powered by two ORTEC 456 High Voltage Power Supplies at an output voltage of 2000V. Also used were two SRS Model SR245 Gated Integrator and Boxcar Averagers. They each had sample rates of 10kHz and sample gatewidths of 15μs. A running average of 100 samples was used for the flame and single sample output was used for the shock tube (and Impulse Facility).

B. Data collection and reduction methods

During data acquisition, the source and emission signals from the gas for both beams were imaged onto the spectrometer entrance slits. The dispersed light from the spectrometer exit slits was projected on to the PMTs. The boxcar averaged PMT signals were recorded with a digital oscilloscope. A temperature change was indicated by two deflections on the oscilloscope; one was a deflection down for the high intensity beam into absorption, and one up for the low intensity beam into emission. Using these deflections and the fact that the brightness temperature of the lamp was known by the setting of the current, the temperature could be calculated.

The calculation of temperature was done using the program under the general name, SODREV.FOR. Two different versions of this program were needed. One was for the flame; the other for the shock tube and Impulse Facility. The reason for this is that in the flame, only one steady-state temperature was measured, therefore only one

temperature calculation was needed. In the shock tube, however, many calculations were needed because temperature was found as a function of time through the shock. Therefore it was necessary to read in from a file the many deflection values. Program SODREV3.FOR for the flame, and SODREV4.FOR for the shock tube are in appendices A and B, respectively. In both programs, the brightness temperature is input and the true temperature and emissivity for that temperature are calculated using an iterative routine and Eq. 6. Then the true temperatures of the two beams are calculated using Eqs. 9 and 10. A prompt is given for the deflections of emission and absorption. With these changes in units of volts from the oscilloscope the temperature of the gas is calculated using Eq. 11. The results of the true source temperature, emissivity of the source, temperatures of the two beams, and gas temperature(s) are then output to a file of the users choice.

IV. Uncertainty analysis

A. Uncertainty corrections

This section is devoted to problems that were identified and dealt with to reduce the uncertainty in temperature measurements.

The first problem that presented itself was the fact that the filament of a tungsten lamp has a temperature gradient across its surface [16]. To deal with this, the filament was examined using a disappearing filament optical pyrometer. It showed that the temperature did indeed vary over the length of the filament, being hottest in the center, and cooler (by less than 50K) at the edges. (Unfortunately, the uncertainty found associated with the optical pyrometer was as much as 25K because the disappearing point is judged by eye. The spectral radiance calibration of the lamp performed by PMEL gave much smaller uncertainty.). Because of this temperature gradient the lamp filament was imaged on the spectrometer slit as in Fig. 4.1.

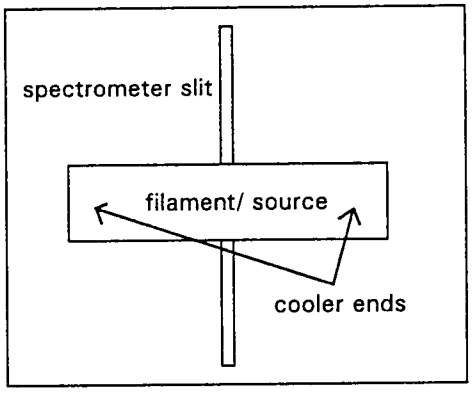


Figure 4.1. Initial Filament Orientation

The second problem was caused by the solution to the first problem. When making line reversal measurements, it is essential that the solid angle of light coming from the source is the same as that coming from the gas [3]. This allows one to omit solid angle calculations. If this is not the case, then one will see more light from the gas than

from the source and the temperature will appear too low. The brightness temperature of the lamp would have to be hotter to make up for seeing extra solid angle from the gas. With the optical arrangement of Fig. 4.1, the source and gas on the spectrometer slit appear as Fig. 4.2.

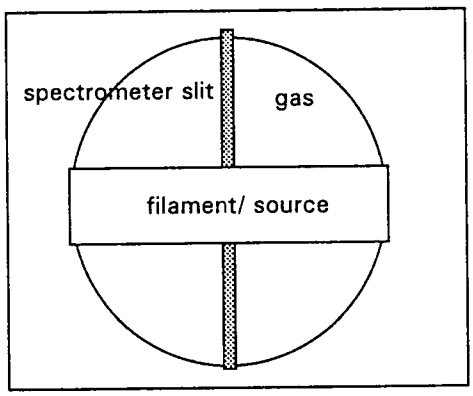


Figure 4.2. Initial Filament Orientation with Gas Image

This is a problem, because as can be seen, the shaded area, imaged onto the spectrometer slit is a component of the signal that does not have a corresponding source solid angle contribution. This gave a temperature of over 100K too high.

As a solution to this, the filament was rotated to align with the slit. This kept the solid angle from the source and gas the same. However, so as not to re-introduce the temperature gradient problem, a shielding face-plate was added to the front of the spectrometer in order to select only the middle portion of the filament. This final orientation is shown in Fig. 4.3. The shaded area represents what is blocked by the face-plate. The temperature gradient in the portion of the filament that is allowed through the face-plate is negligible. It could not be discerned with the optical pyrometer.

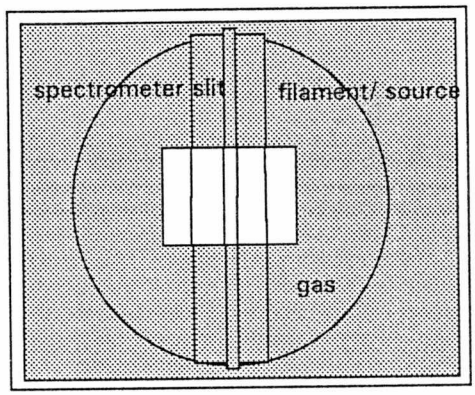


Figure 4.3. Final Filament Orientation

With this orientation, the first problem is solved. The filament is observed to have the same temperature across this region. The second problem appears to be solved; however to assure that the same solid angle is received by the spectrometer from the source as from the gas, some calculation is necessary. The face-plate has a dimension of 4mm for one spectrometer and 5.5mm for the other. It must be assured that the source and gas both completely fill this height. This requires that an aperture be used in the path and that the aperture limit both the gas and the source. To do this, a calculation of the size of the fully-lit image must be made [3]. This calculation includes the object and image distances, the focal lengths of the lenses, and the size of the aperture that is used in the path. Results of the calculation require that the apertures be less than 4.29cm for beam one and less than 4.12cm for beam two. The necessary equations and a derivation of them appear in Winkleman [3] and will not be repeated.

B. Optical and electronic systems

The optical systems include the lamp and all of the optics used. There are calibration uncertainties involved in all of them. The method of uncertainty reduction involves propagation of errors [17]; as an example of the method, Eq. 4 will be used.

In this equation the only source of uncertainty is due to the spectral radiance, L_W. Therefore the percent uncertainty for T_B in Eq. 4 is given by the square root of Eq. 12

$$\frac{U_{T_B}}{T_B} = \frac{1}{T_B}\frac{\partial T_B}{\partial L_W} U_{L_W}, \qquad (12)$$

where U_i stands for the uncertainty in i. Using this method, the uncertainties for more complicated equations such as T_1, Eq. 9 can be calculated, by adding squares of partial derivative terms and taking the square root to obtain the overall uncertainty.

The optical uncertainty values are given in table 4.1.

Table 4.1. Optical Uncertainty Values

Symbol	Description of Symbol	Uncertainty (+/- %)
L_W	spectral radiance	7.5
ε	emissivity	0.905
τ	trans. coef. of lamp window	2.15
τ_L	trans. coef. of all lenses	2.15
τ_W	trans. coef. of shock tube window	2.17
ρ_{M1}	refl. coef. of mirror one	2.17
ρ_{M2}	refl. coef of mirror two	0.51
ρ_{bs}	refl. coef. of beamsplitter	3.0
τ_{bs}	trans. coef. of beamsplitter	3.0

The uncertainty in the spectral radiance was specified from the calibration of the lamp done by PMEL, AEDC. The uncertainty in the beamsplitters is taken from the calibration performed when they were made by PMEL. Uncertainty in the emissivity is from both

that quoted in the literature in which the values were found and from the variation between sources. The uncertainties in the transmission and reflection coefficients of the lenses, mirrors, and windows are from the catalog specifications for their material. These values combine to give an optical uncertainty of +/- 0.81%. This is the uncertainty in the temperatures of the beams as calculated from the spectral radiance of each. The beams pass through many optical components and incur many losses before the test volume is reached. This optical beam uncertainty accounts for the uncertainties in the optics. It corresponds to about +/-18K at 2000K.

The electronic uncertainty is given by the signal to noise ratio. This varied a great deal depending on the situation, from one-to-one to ten-to-one. However, most of the time it was approximately five-to-one. This signal to noise ratio is taken as the uncertainty in the deflection for absorption and emission. Therefore the final uncertainty is given by applying Eq. 12 to Eq. 11 for the uncertainties in the two beam temperatures and the deflections, 'a' and 'e'.

C. Final uncertainty values

The final uncertainty values for the gas temperature, calculated as explained in the previous section are presented in table 4.2 for various signal-to-noise ratios.

Table 4.2. Temperature Uncertainty Values

S/N	Percent (+/-)	Temperature @ 2000 K
10:1	0.646	13
5:1	0.818	16
2:1	1.56	31
1:1	2.96	59

V. Application of method to flat-flame burner

A. Description of burner

The McKenna Products Standard Model flat-flame burner has a porous stainless steel surface with a shroud ring for introducing a heat/fuel shielding gas (nitrogen). Cooling of the burner is accomplished by constantly flowing water through copper coils imbedded in the porous surface of the burner [18]. Burner operation provides a flame just above the surface (about 5mm) and at steady state conditions. The gases, in this case nitrogen and oxygen in an air combination, and methane for the fuel are pre-mixed before entering the burner, requiring only one test gas inlet. The pre-mixing of the gases is done by first routing each gas to a read-out panel, where the flow of each gas is regulated separately by orifices in the gas lines. The flow rate of each gas can be controlled using regulators on the gas bottles, and the flow rates are read out on the panel. The mixture is then delivered to the burner through one line.

B. Optical arrangement

The experimental set-up for the flat flame burner is shown in Fig. 5.1.

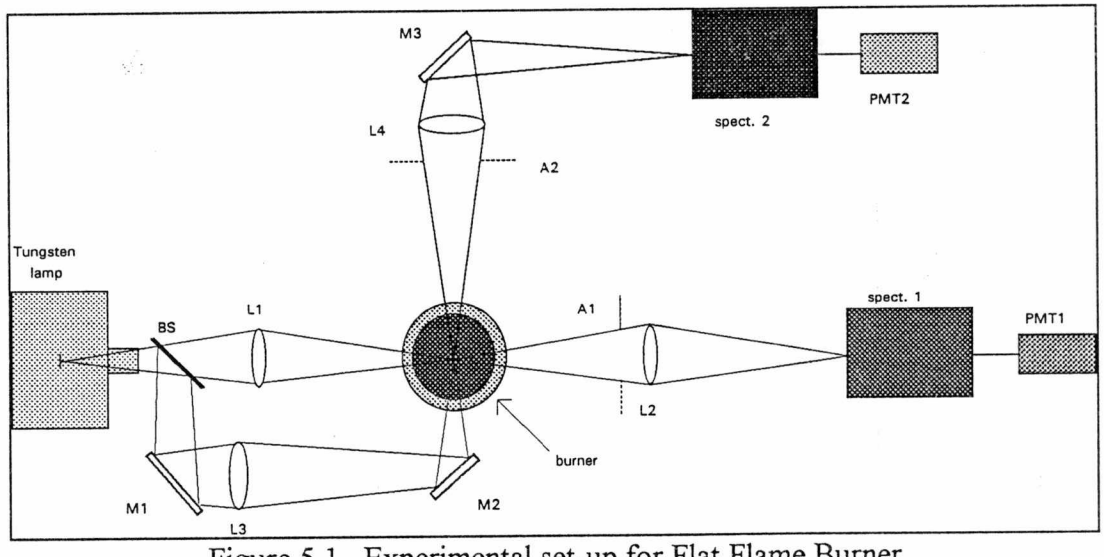
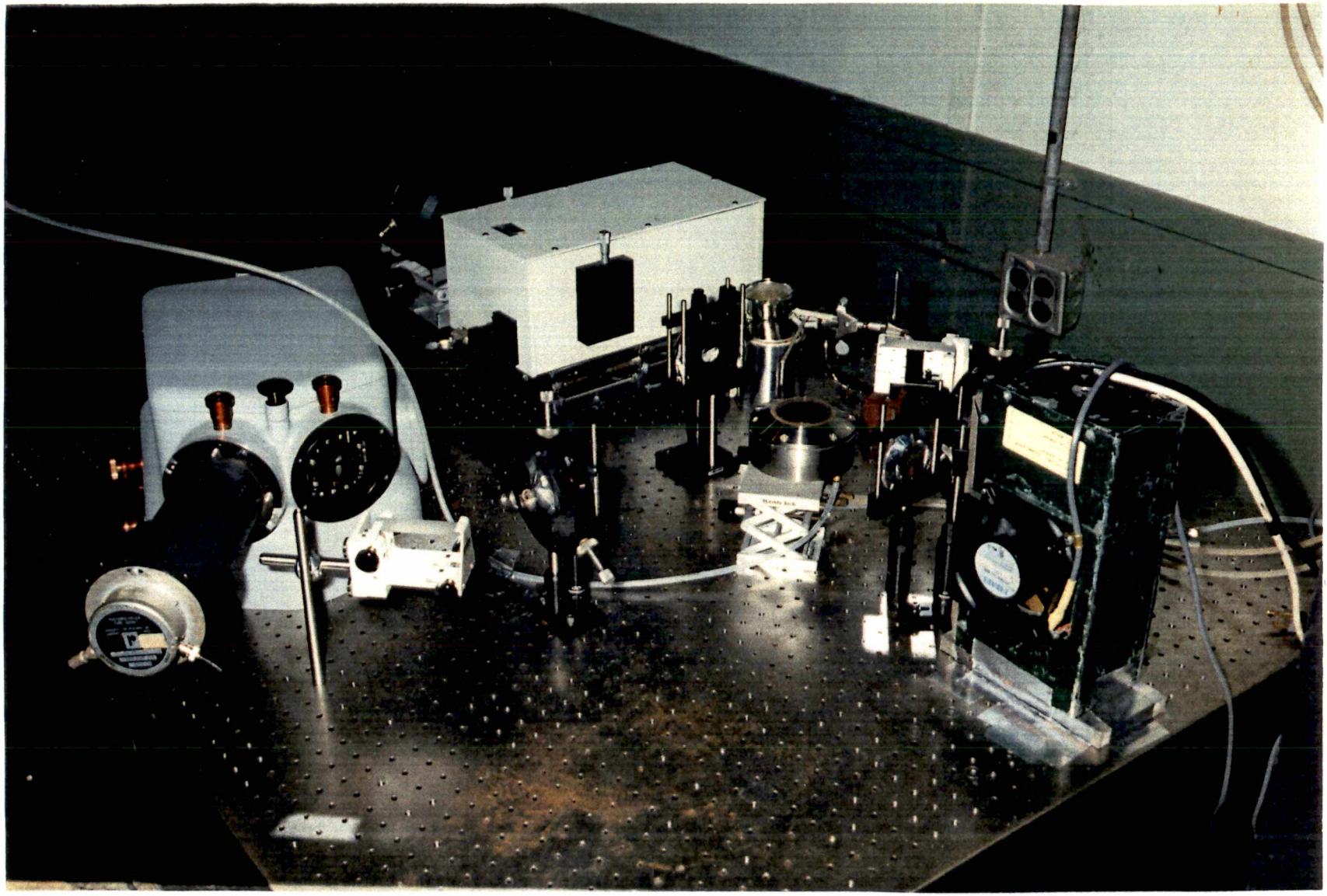


Figure 5.1. Experimental set-up for Flat Flame Burner
(view from top with safety hood removed)

In Fig. 5.1, L1 and L2 are lenses of focal length 90mm each, and L3 and L4 are lenses of focal length 170mm each. They were chosen both for the necessary optical arrangement and because of availability. M1, M2, and M3 are mirrors. BS is a beamsplitter of reflectance/transmittance 20/55 to give the two beam paths different intensities and, by Eq. 4, different temperatures (about 200K). A_1 and A_2 are apertures to ensure that the solid angle from the flame is equal to that from the lamp, which is necessary to eliminate the problems of chapter IV, section A [3]. These apertures were also used to nullify differences between the two spectrometer-PMT-boxcar systems. The beamsplitter was replaced by one of 40/31. (Because the beam paths are slightly different, the optics cause different losses for each path. Therefore the beamsplitter, 40/31 was needed to obtain a split of 50/50 at the entrance of the spectrometers.) Then the signal was measured using both systems, adjusting the apertures so that the signals and changes in signal were the same for each of the two systems. The 20/55 beamsplitter used for data acquisition was then re-inserted in place of the 40/31. This nullification was repeated at the beginning of each day of experimentation, as without it, the temperature could not be calculated as a direct ratio of the signals of emission and absorption. Because the relative signals did not change appreciably from one day to the next, it was assumed that adjustments during the day were not necessary.

The experimental set-up can be seen more readily in the photograph on the following page. The burner can be seen in the center. The two spectrometers are to the left (spect.2) and rear (spect.1). The housing of the PMT can be seen attached to the front of spect.2. The PMT for spect.1 is attached behind the spectrometer, and is just visible in the shadows. The tungsten lamp is on the far right, with cables from it going to its power supply. To the left of the burner, the nitrogen shroud supply can be seen coming from the left, over the top of spect.2. The inlet gas supply and water circulation tubes are coming from the right and can be seen leaving the photograph to the right of the lamp.



C. Introduction of sodium to the flame

The sodium was introduced to the flame in three ways. In all three cases, sodium was in the form of sodium chloride, NaCl. Two of the ways gave a short lived (2-3 minutes) sodium presence in the flame, one a long-lived (20-25 minutes) presence. It would seem that the long-lived method would be the obvious best choice for the introduction; however, it had rather bad side effects.

The first method was to dissolve the salt in water to saturation. The solution was sprayed into the flame using a 'plant spritzer'. This method gave short-lived sodium. Also, the effects of the presence of water in the flame are unknown. It was a feasible method for introduction; however for calibration of the system and extended temperature measurements a method of longer duration was pursued.

The second method was to leave a screen in the aforementioned saturated solution overnight. The salt crystallized on the screen. The screen was placed at a height of about 5mm from the burner surface during burner operation. This gave even shorter lived sodium presence. As an added argument against this method, it also introduced significant amounts of soot from the screen into the flame, which caused optical problems due to transmission loss, in addition to a short lifetime.

The last method used, and the method used for most of the experiment, was to deposit the salt onto the burner surface in solid form. This gave a lifetime of 20-25 minutes and allowed for precise control of the amount of sodium introduced to the flame. However, there was a side-effect that was discovered after the experiment had finished. The deposition of solid salt caused the flame to sink down onto the surface of the burner. The fact that it usually floats above this surface is what allows the burner material to handle the high temperatures achievable with a burner of this type. With the surface directly exposed to the flame, the surface warped, became discolored, and developed spikes that ruined the porous surface of the burner beyond repair. Because of this, it may

not be the best seeding choice. The gains in sodium content stability and lifetime must outweigh the necessary burner replacement after performing the experiment. Method one, after examination of the effect of the presence of water, would probably be a preferable choice.

D. Determination of expected temperature

The expected temperature was examined for an equivalence ratio, Φ, of 1.0. The equivalence ratio is the ratio of the amount of oxygen that is needed in the flame to burn the amount of fuel present (stoichiometric condition), to that amount of oxygen which is actually present in the flame [1]. Therefore, if there is more oxygen than is necessary in the mixture, the flame is said to be lean and the equivalence ratio is less than 1.0. When the mixture has an equivalence ratio of 1.0, the flame is at its highest temperature. An equivalence ratio of 1.0 was easy to attain in the experimental set-up, as will be evident in Sec. E.

Two methods were used to determine the temperature that was expected from the air-methane flame. The first was a platinum-rhodium/platinum, or Pt10Rh-Pt thermocouple. The bare wires were covered with a ceramic compound for heat shielding. It was referenced to $0^{o}C$ using an ice bath. The thermocouple leads were connected to a voltmeter and the temperature was obtained from tables for these particular thermocouple materials [13]. This thermocouple is specified for prolonged use between 220K and 1550K. However, it can reach 1850K for short periods of time [19]. The thermocouple was suspended over the flame using a clamp. It was placed so that it was at the same height above the surface of the burner as the source light passing through the flame.

Because the temperatures being read were above these specifications, a radiative correction factor was necessary. The thermocouple was radiating in the orange-yellow, which corresponds to a temperature loss of about 525K +/-20K [20]. With the flame

operating at an equivalence ratio of 1.0, the thermocouple measured 1510K. When the radiative correction is accounted for, this gives a temperature of 2035K +/-20K. This does not take conduction losses into account.

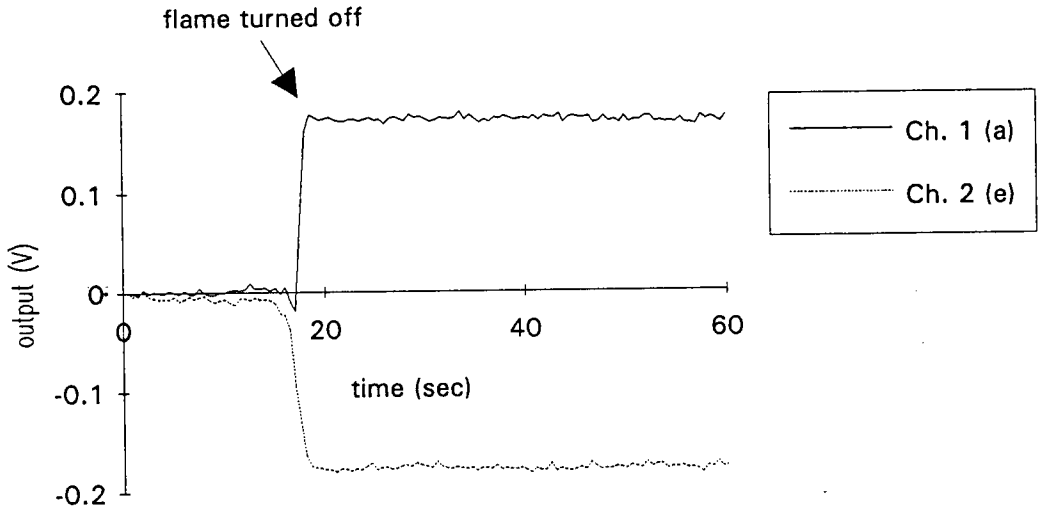
The second method for determining the expected temperature was by computer calculation. NASA SP-273 Chemical Equilibrium Program is a program used to calculate equilibrium temperature and equivalence ratio of flames using concentrations of the gases put into the flame. It was set up to perform a temperature calculation for average gas flow-velocity of an air/methane flame at an equivalence ratio of 1.0 [21].

This program gave as output a temperature of 2275K. However, this number also needs adjustment. The program calculates the temperature of a perfect flame, with no outside effects, at equilibrium. This, unfortunately, is not the case for the experiment. The flame is near equilibrium, within the uncertainty allowance, but there is loss due to the cooling of the burner surface. The actual temperature, at just under 1cm above the surface of the burner was found to be lower than the equilibrium temperature by 182K to 257K (taken here as 220K +/- 35K) [2]. This gives a final temperature for this method of 2055K +/- 35K. (Cattolica, [2], used a burner very similar to the one used in this experiment. He compared radiation corrected thermocouple data to theoretical models, and in support of comparison of this work to his, at Φ=0.9, he obtained an equilibrium calculation of 2132K. The calculations done in support of this experiment gave at Φ=0.8, T=2004K, and at Φ=1.0, T=2275K [2]. These correspond as they should.)

E. Experimental results and comparison to calculated results

Experimental results were obtained according to Chap. III, Sec. B. One departure from that method is that the trace was begun with the flame on and then the flame was turned off. Therefore, in the traces, channel 1 is coming up out of absorption and channel 2 is coming down from emission. These level differences are taken as the deflection

values for program SODREV3.FOR. A typical trace for oscilloscope output, followed by a portion of the output from SODREV3.FOR can be seen in Fig. 5.2. The gas temperature is at the bottom of the figure.



Output of Sodrev3.for

TMAX	ETMAX	TMIN	ETMIN
2400.0	0.4392	2200.0	0.4422

TB = 2111.3

EMIS	Tt	T1	T2
.44095	2287.5	2138.7	1950.1
.44089	2287.6	2138.8	1950.1
.44089	2287.6	2138.8	1950.1

deflections (mV)

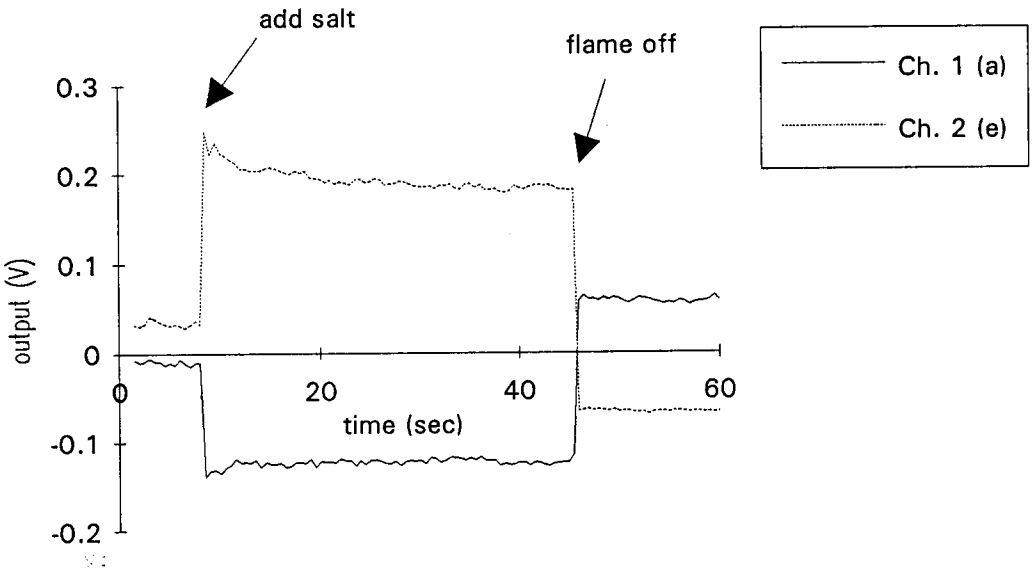
a: 169.88 e: 169.77

TG = 2044

Figure 5.2. Typical Flame Trace and Calculation Output

Prior to shock tube experiments, it had to be shown that the temperature measurement was independent of the amount of sodium in the path. This was shown

during work on the flame by taking a measurement with very little salt and then adding more salt to the flame. The expected result is that the signal will change by a great deal, but that the two temperature calculations with these two sets of deflections will not change. The results of one of these trials are presented in Fig. 5.3.



Output of Sodrev3.for

1st Na amount				2nd Na amount			
TMAX	ETMAX	TMIN	ETMIN	TMAX	ETMAX	TMIN	ETMIN
2400.0	.4392	2200.0	.4422	2400.0	.4392	2200.0	.4422
TB = 2111.3				TB = 2111.3			
EMIS	Tt	T1	T2	EMIS	Tt	T1	T2
.44095	2287.5	2138.7	1950.1	.44095	2287.5	2138.7	1950.1
.44089	2287.6	2138.8	1950.1	.44089	2287.6	2138.8	1950.1
.44089	2287.6	2138.8	1950.1	.44089	2287.6	2138.8	1950.1
deflections (mV)				deflections (mV)			
a: 69.2		e: 104.43		a: 179.46		e: 258.75	
TG = 2064				TG = 2062			

Figure 5.3. Independence of Temperature on Sodium Amount

Provided the amount of sodium is sufficient to establish an emitting/absorbing medium, but not so much that transmission problems are introduced, Fig. 5.3 makes it clear that the temperature is independent of the amount of sodium. The two temperatures differ by only 2K, well within the uncertainty allowance from Chap. IV, Sec. C of 13K for a S/N of 10:1.

Now, to compare the experimental results to those obtained with the thermocouple and the computer calculation, an equivalence ratio of 1.0 must be attained. This was done with the knowledge that at Φ=1.0, the temperature of the flame is at its maximum value. To find this point, the flow rates for oxygen and nitrogen were set for an air mixture, about 20% oxygen and 80% nitrogen. (These settings, as well as the control of the methane content, had repeatability errors which were not outside the calibration error of the system, so they were not taken into account.) The methane was added next. It was added quickly at first to start the flame burning to keep too much unburned methane from escaping into the room. The methane flow rate was gradually increased, in steps, recording deflections along the way. The results of three of these runs are represented in Fig. 5.4. From this, Φ=1.0 can be taken as the highest temperature point on each series. The differences in each of these runs in Fig. 5.4 could be due to the repeatability uncertainty in the gas content. A concentration of 80% nitrogen and 20% oxygen, an air mixture, was desired, but if the amount of nitrogen was too high (greater than 80% compared to oxygen),the temperature will appear low (compare Run 1 to Run 2). Also, if the ratios of nitrogen and oxygen were correct, but their total volume were lower, it would take less methane to achieve an equivalence ratio of 1.0 (compare Run 1 to Run 3). The coarseness of data acquisition, due to coarse gas bottle regulator control, may have caused differences as well. However, for all three, the differences are within the uncertainty allowance from Chap. IV, Sec. C, for a S/N of 10:1.

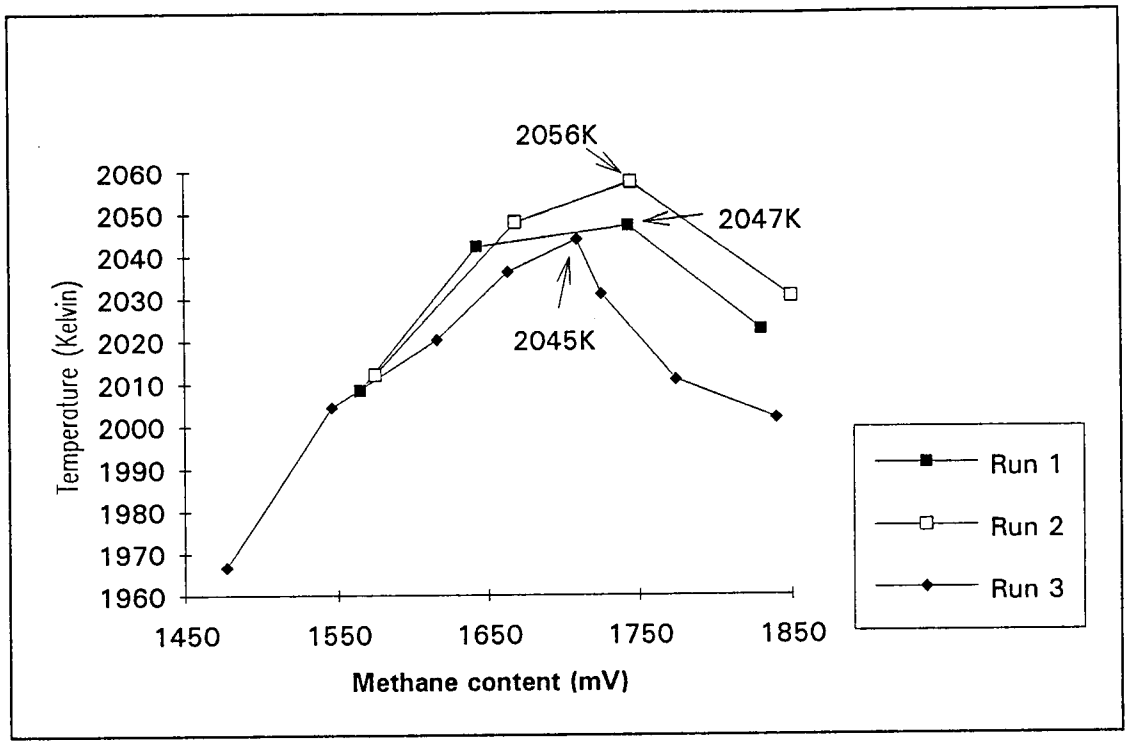


Figure 5.4. Temperature versus Methane Content

Comparison of the expected and experimental temperatures is favorable. These are given in Fig. 5.5 along with the uncertainty ranges. The central value for the experimental result is taken as the average of the three runs in Fig. 5.4. The measured value for the thermocouple is given; the uncertainty of the radiative correction factor is from the difficulty in knowing the exact color at which it is radiating. However, the actual temperature may be higher than that which is given because it does not take conduction losses up the wires of the thermocouple into account, but from Fig. 5.5, it can be seen that SLR produces a temperature measurement matching, within the uncertainty calculation, that which is expected.

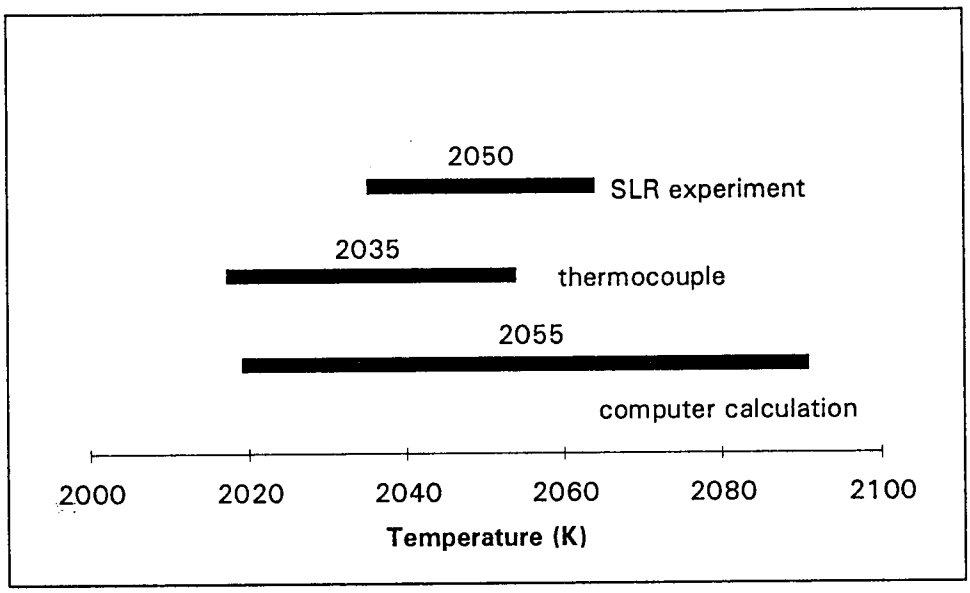


Figure 5.5. Comparison of Calculated and Measured Temperatures

VI. Application of method to shock tube

A. Description of shock tube

The shock tube used for the move to time-resolved measurements is shown in Fig. 6.1.

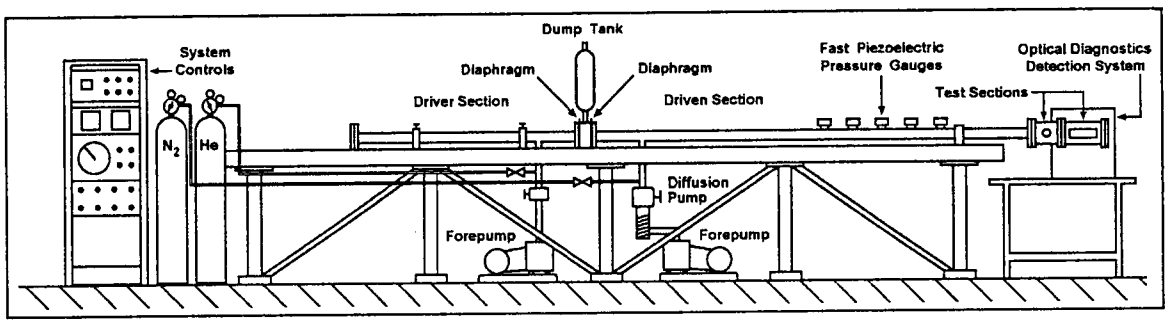


Figure 6.1. Shock Tube Diagram

As can be seen, the shock tube consists of three sections. The high-pressure driver section, on the left, is filled with helium. The low pressure driven section, on the right, is filled with the test gas, which is room air in this case. The section between the two diaphragms, in the middle, is filled with helium to an intermediate pressure.

When the shock tube firing sequence is initiated, a switch on the system control panel causes a valve between the intermediate pressure gas and the dump tank to open. The dump tank is initially at or near vacuum; therefore opening the valve causes the pressure to drop quickly in the middle section. This causes the diaphragm on the left to rupture. The high-pressure gas propagates to the right, bursting the diaphragm on the right. This initiates a shock wave which moves down the shock tube.

While the shock wave is propagating toward the test section on the right, it is detected by pressure gauges (Kistler 603B1 transducers and 5004 charge amplifiers) in the driven section. Their detection signals are fed to a data acquisition program and are used to calculate the velocity of the shock and to provide triggers to the diagnostic instrumentation.

The arrival of the shock at the test section windows is referred to as the incident shock. This shock wave moves past the test section windows and then hits the back wall of the tube. It reflects back across the test section windows as what is referred to as the reflected shock. The reflected shock further heats the gas above the temperature of the incident shock. The temperature drops drastically with the arrival of the helium driver gas at the test section. The entire operation, from throwing the switch on the system control panel to arrival of the helium, takes about 100ms. Bursting of the right diaphragm to arrival of the helium takes 3ms. [22, reference for entire section]..

B. Optical arrangement

The experimental set-up for the shock tube is shown in Fig. 6.2.

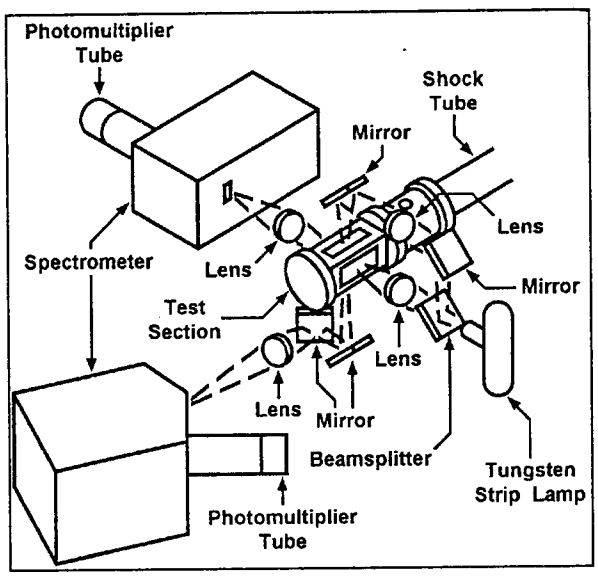


Figure 6.2. Experimental Set-up for Shock Tube

The beam path used is very similar to that of the flat-flame burner of Chap. V, Sec. B. Most of the same optics are used. The difference is that, because of limited space, the beam path had to be folded rather than being rectilinear. This necessitated the use of two

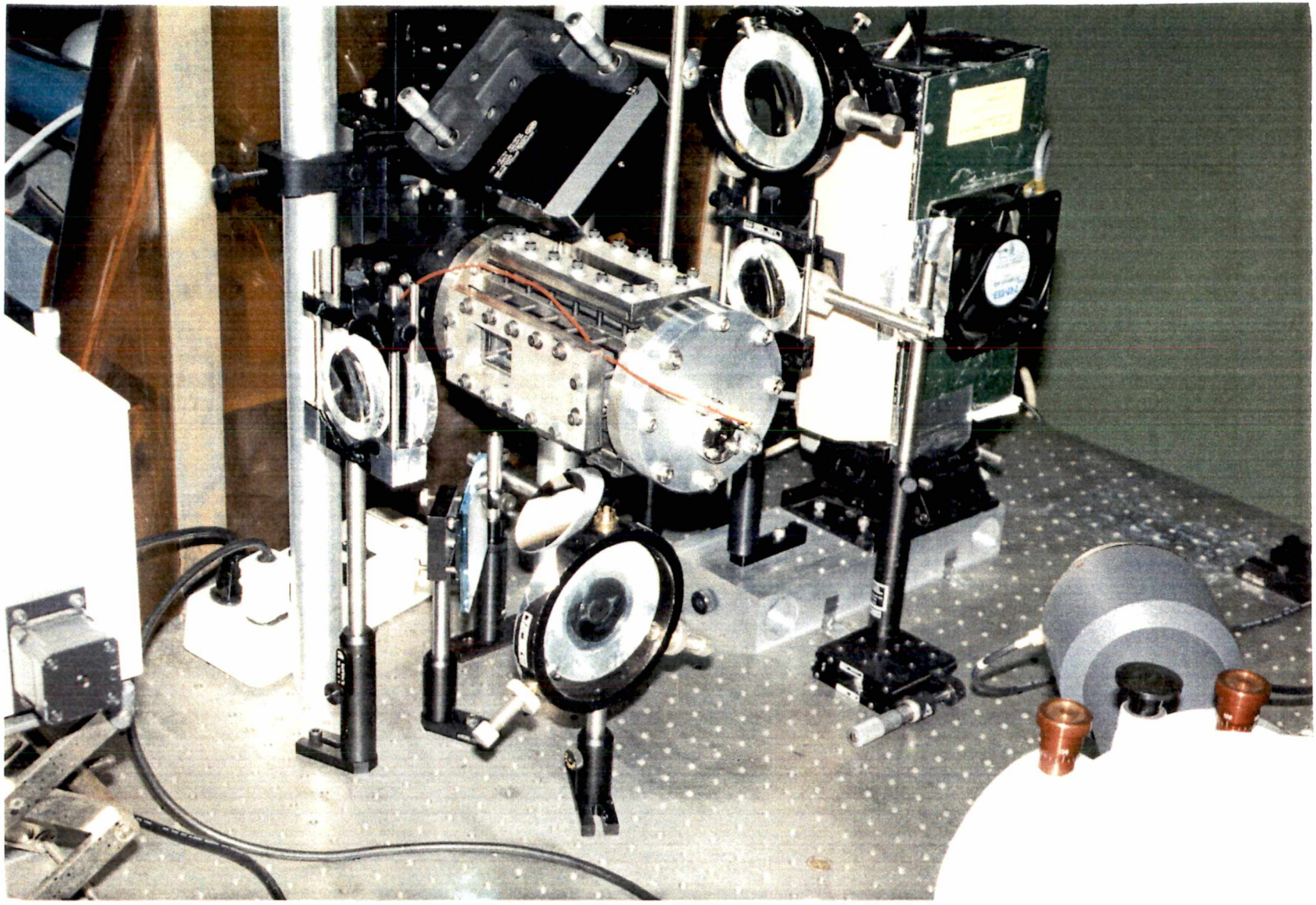
additional mirrors below the test section, and some rather tight optical turns. The apertures that are necessary in the beam path to eliminate the problems of Chap. IV, Sec. B and nullify the differences in the systems are not shown in this diagram, but they are present just to the test cell side of the spectrometer collection lenses.

The experimental set-up can be seen more readily in the picture on the following page. The test section is in the center of the picture. The spectrometers are partially on the page, being to the far left and lower right of the picture. Attached to the spectrometer on the lower right, is the PMT housing. The apertures are taped to the lens holders just to the test cell side of the collection optics. To the far upper left, in blue, is the shock tube leading to the test section.

From this view, the shielding at the lamp can be seen. The front of the lamp has a quartz protrusion with a window at the end that is parallel to the tungsten filament. This is the point of light exit from the lamp. The protrusion keeps metallic tungsten from depositing on the exit window through which the filament is viewed. Without sufficient shielding, light from the lamp would escape through the sides of this 'snout'. This light would be allowed to escape into the system causing an error in that the temperature would be viewed as too high. Also, because the lenses used are larger than the beamsplitter, this excess light would make it through the lens, but not through the beamsplitter, also causing the temperature to appear too high. Therefore, the shielding was used to allow only the light from the front parallel window to escape. The transmission loss from the light going through the quartz window is included in the temperature calculations.

C. Introduction of sodium to the shock tube

Three methods were used for introduction of sodium to the shock tube. Again, sodium in the form of table salt was used. Two of these methods gave good results, one



better than the other. The other method gave very poor results, and it is not recommended.

As an aside, before sodium was introduced to the shock tube for the first time, several background shots were made to check for any shock-generated light in the region of 589nm. It was found that there was no emission in this region that could interfere with the data acquisition.

The first method used salt in solid form. The salt was ground with a mortar and pestle to a fine powder. It was placed in the shock tube about half a meter from the test section using a metal rod for placement. The correct amount of sodium was found by trial and error, and the entire tube was cleaned between runs. It was found that only about 10mg was necessary to get a very good signal and good results. If too much salt was used, transmission problems occurred and the tube became difficult to clean. This method gave the best results of the three tried and was also the easiest to use.

The second method used was to place a small amount of a saturated solution of salt and water at the same place in the shock tube. Very poor results were obtained, principally because of optical transmission problems caused by water vapor. Even using only 0.1ml of the solution, arrival of the shock reduced the transmission to zero for the duration of the oscilloscope sweep.

An additional problem was that the presence of water vapor caused errors due to changed initial gas conditions. Its presence caused a change in the specific heat ratio, $C_p/C_v=\gamma$, of the gas. This altered the sound speed, a, in the shock tube given by (ideally),

$$a = \frac{\gamma P}{\rho}, \qquad (13)$$

where P and ρ are pressure and density, respectively. The program that calculates the shock velocities and controls the diagnostic triggering depends on the initial gas conditions of the high and low pressure sections of the shock tube for its calculations. Therefore, during most of the runs using a water solution, velocities were calculated incorrectly and if triggers ever even occurred, they were at the wrong time. This method of sodium introduction is not recommended.

The third method of sodium introduction was to place a saturated solution of methanol and salt at the same location. This gave good results, though not as good as with the solid form. The problems present with the water vapor were not an issue here because methanol evaporates more readily. Using 0.1ml of the solution gave good temperature measurements, but the signal and S/N were low. However, much more of the methanol again introduced transmission problems similar to those for the salt/water form. This method of introduction was also more difficult and messier than using solid salt powder.

D. Additional instrumentation for timing and triggering

Timing and triggering were accomplished using the pressure transducers in the driven section of the shock tube. They were only used as sensors, not actual pressure measuring devices. The signal they generate when the shock front passes them is fed to the system that calculates the shock velocities. It was also used as a positive going trigger pulse. There are six of these transducers. Five are equidistantly located along the tube and one is at the end wall. Referred to as K1-K6, the ones used for SLR triggering were K5 and K6.

The signal from K5 was used to trigger the Lecroy 9310 oscilloscope, which was set up for a sweep time of 5ms, ranging from t=-0.5ms to t=4.5ms. This trigger occurs approximately 1.1ms before the incident shock arrives at the test cell window. This signal

was used to monitor the long-term effects in the flow. These include any transmission loss that remains after the flow has ceased, such as those caused by deposits on shock tube windows. The trace began before the arrival of the incident shock and ended after the arrival of the helium driver gas.

The signal from K6 was used to trigger the Lecroy 9314A oscilloscope, which was set for a sweep time of 1.0 ms, ranging from t=-0.1ms to t=0.9ms. This signal occurred approximately 1.2ms after the K5 trigger, or about 0.1ms after the arrival of the incident shock at the test cell window, and was used to begin the oscilloscope trace for the reflected shock duration. The trace began just before the reflected shock was established and ended after the arrival of the helium. Beginning the sweep before the arrival of the K6 signal with a pre-trigger (thus the negative time range) provided, along with the signal trace from the K5 trigger, a measure of the noise for uncertainty comparison regarding signal-to-noise ratio. It is taken from the fluctuation in the signal before the shock front arrived.

An examination of the traces triggered by K5 shows that at the appropriate time, these traces match those triggered by K6, as they should. Therefore, in the event that K5 gives a trigger, but for some reason, K6 does not, the K5 trace can be used for temperature measurements.

E. Determination of expected results

The expected shock tube temperatures were calculated by computer from flow equations derived in reference [23]. Parameters needed for the calculations are the initial pressures, gas specific heats for the test and driver, and the conservation equations of mass, momentum, and energy which are present in the shock tube. The conservation equations, Eq. 14, are given in shock-fixed coordinates: the shock front is at rest [11].

$$\rho_1 u_1 = \rho_2 u_2$$
$$P_1 + \rho_1 u_1^2 = P_2 + \rho_2 u_2^2 \qquad (14)$$
$$H_1 + \tfrac{1}{2} u_1^2 = H_2 + \tfrac{1}{2} u_2^2$$

Subscripts 1 and 2 represent the gas entering and leaving the shock front, respectively. The symbols H_i, P_i, u_i, and ρ_i represent the enthalpy, pressure, velocity, and density in the shock-fixed coordinates, assuming unit mass. The conservation of energy equation assumes no heat exchange in the shock wave, which is a valid assumption [11]. These equations are used to define the incident shock. When the incident shock parameters are known, the reflected shock properties can be calculated [23].

For the M=4.0 case of interest, the calculated vibrational temperatures for the incident and reflected shocks are shown in Fig. 6.3, where the arrows point to the beginning of the incident and reflected shocks [23].

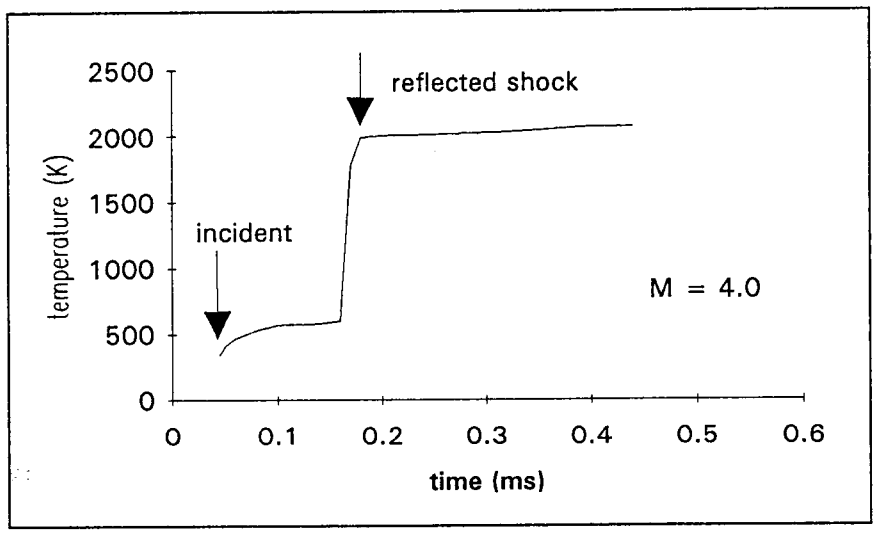


Figure 6.3. Calculated Shock Tube Temperature

The beginning of the incident shock exhibits the non-equilibrium process of vibrational excitation of the molecules. However, since the reflected shock wave is in a state of

equilibrium nearly from the time of its inception, this vibrational temperature can be assumed to be the same as the electronic excitation temperature that SLR measures [1]. The final equilibrium temperature of the reflected shock is about 2070K.

This figure also gives an indication of the useful test time. From the figure, the reflected flow lasts for about 250μs. Therefore, Fig. 6.3 gives information about the temperature of the reflected shock and the duration of its conditions.

Another method is currently being used for measurement of the useful test time. This diagnostic technique detects the arrival of the cool helium driver gas [24], and is based on laser Rayleigh scattering. An argon ion laser, tuned to a molecular iodine transition, is projected as near to coaxial to the flow centerline as is possible. Scattered light from particles in the test area is focused through a cell filled with iodine and onto a PMT. The iodine filter is used to filter out the wavelength of the incident laser light, so that just the scattered light is collected. When the flow passes through the viewing area, the scattered light is Doppler shifted from the iodine transition, and the signal is detected by the PMT, signaling the arrival of the shock. When the helium arrives, there is a sharp decrease in signal because the Rayleigh scattering cross section of helium is so much smaller than that for air, thus the scattering is less. After the helium arrives, the signal remains elevated from the baseline before the shock arrives, because the density of the test volume has increased over that from the beginning, and the flow is still moving for a small time afterwards. An oscilloscope trace from a shock tube shot is shown in Fig. 6.4 [24].

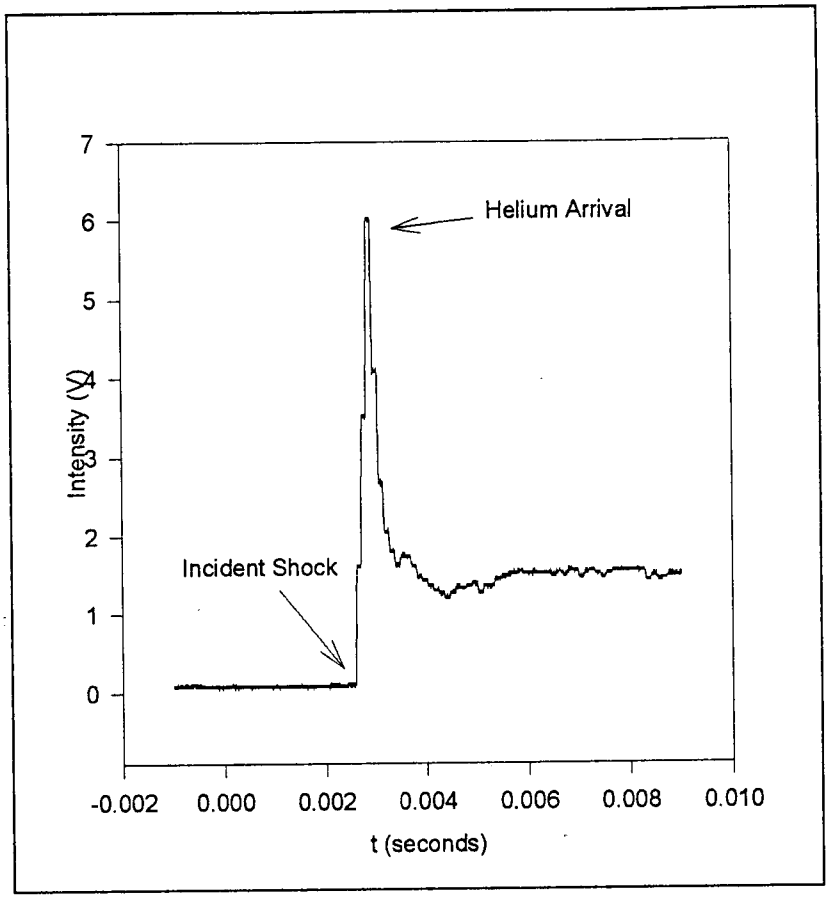


Figure 6.4. Helium Arrival in Shock Tube

The incident shock and arrival of helium are marked in Fig. 6.4. The incident and reflected shocks cannot be distinguished because of the resolution used, but this could be improved with a higher resolution recording system. The oscilloscope trace is triggered (t=0) by K1, the first pressure transducer. From the figure, the test ends and the helium arrives at about 3.5ms after the K1 trigger.

F. Experimental results and comparison to calculated results

Whereas the flat-flame burner temperatures were considered steady-state, it was desired to measure time-dependent temperatures in the shock tube. With the exception of the case in Fig. 5.3, where the amount of sodium was changed and the temperature was measured twice, one oscilloscope trace was used for each flame temperature

measurement. It was necessary to obtain a baseline signal (source only) prior to each shock tube firing. Deflections for the emission and absorption were measured point-by-point on the oscilloscope trace and were input as a file to SODREV4.FOR, and a file of temperatures versus time was output to another file.

Experimental results are presented for two of the three sodium introduction methods used. Due to optical transmission problems discussed earlier in this chapter, results for the salt-water solution could not be related to temperature. First, for the case of the salt-methanol solution, the solution was added in the amount of 0.1ml, introduced by pipette. The shock tube driver and driven gas pressures were set to produce a shock of about Mach 4. The oscilloscope absorption and emission traces and resultant temperatures versus time for Run 18 are given in Fig. 6.5.

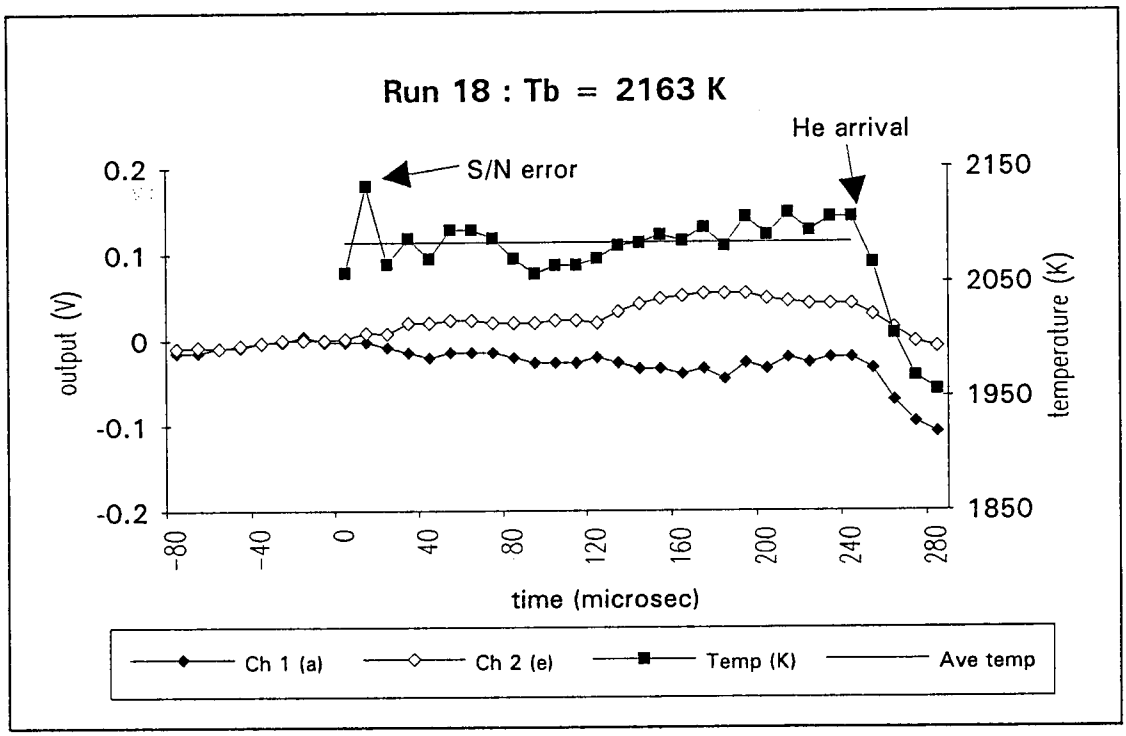


Figure 6.5. Shock Tube Temperature Measurement Using Salt-Methanol Solution

Signal traces triggered from pressure transducers K5 and K6 were identical from the K6 trigger time on; Fig. 6.5 is a truncated version of the K5 triggered trace. The deflection and temperature values are shown on the y-scales to the left and right, respectively. The noise level for the entire trace is given by the level indicated at t=-80μs, which corresponds to the signal level for the K5 triggered trace before the time of the K6 trigger at t=0. The noise level is needed to indicate how the S/N ratio influences the uncertainty of the temperature measurement. In Fig. 6.5, one point is noted as including a S/N error, which causes it to vary greatly from the average temperature. As can be seen from the deflection traces, the signal here is no bigger than the noise level, indicated at t=-80μs. This low S/N ratio causes the temperature measurement to be a departure from the average temperature (solid line) of 49K, the average temperature being 2085K. However, from table 4.2, this does not exceed the allowed uncertainty for S/N of 1:1, which is 59K.

Moving along the trace, the S/N level is about 2:1 for the time between 40μs and 120μs, giving an allowed uncertainty of 31K. For the points between 140μs and 200μs, the S/N level is about 3:1, and the temperature trace at this time matches the average temperature much more closely. The maximum temperature deviation from the average is 27K for the low temperature point, near the center of the trace, and this is within the allowed uncertainty for the S/N level that is present.

The sudden temperature drop at 245μs after the K6 trigger was caused by arrival of the cool helium driver gas. From the pressure transducer data acquisition program, it is known that the time between the K1 and K6 triggers was about 3420μs. Therefore the helium arrival was 3665μs after the K1 trigger.

An experimental result, Run 6, for the case where solid sodium was placed in the shock tube is given in Fig. 6.6. Approximately 10mg of salt was added, and the shock tube was again configured for a shock of Mach 4.

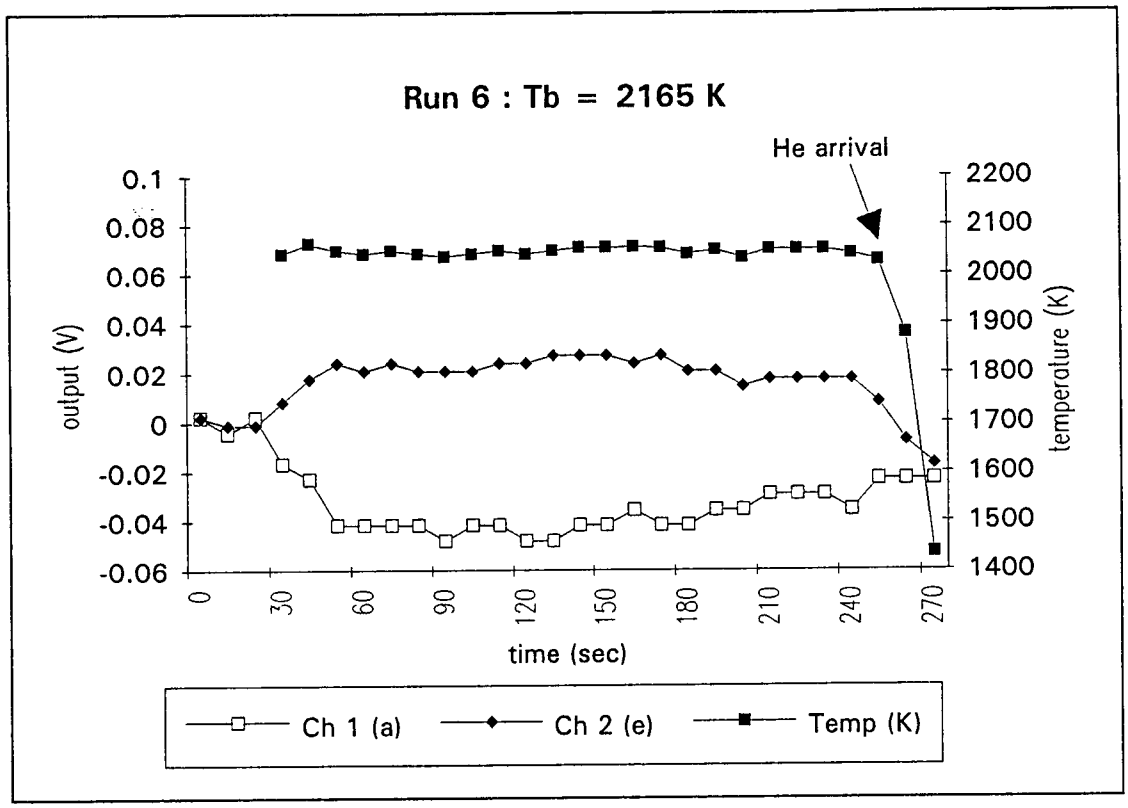


Figure 6.6. Shock Tube Temperature Measurement Using Solid Salt

This trace is triggered by the K6 transducer, defining the t=0 time. The noise level viewed in the corresponding trace from the K5 trigger was comparable to the level shown in Fig. 6.6 before establishment of the emission at 20μs. The signal levels from the oscilloscope are noticeably higher than in the methanol-salt case, Fig. 6.5 and, since the noise levels are the same for both cases, a lower temperature uncertainty exists. The S/N level, taken as 5:1 throughout the trace, results in an uncertainty of 16K, and the largest departure from the average temperature of 2047K is 14K at t=200μs.

The helium arrived 250μs after the K6 trigger, corresponding to a helium arrival time of 3665 μs after the shock was detected at K1, since the time between K1 and K6 triggers was 3415μs.

Comparison of these data to those which were calculated involves two things: the comparison of temperature and helium arrival time. Runs 18 and 6 both have arrival times

of 3665μs after the K1 trigger. (The fact that they are *exactly* the same is likely a coincidence.) This value compares well to the 3.5ms arrival time estimated from the graph in Fig. 6.4. A better comparison is not possible due to the low time resolution in Fig. 6.4.

Regarding temperatures, however, the comparison is more involved. The average temperatures, uncertainty ranges, and expected temperature are compared graphically in Fig. 6.7.

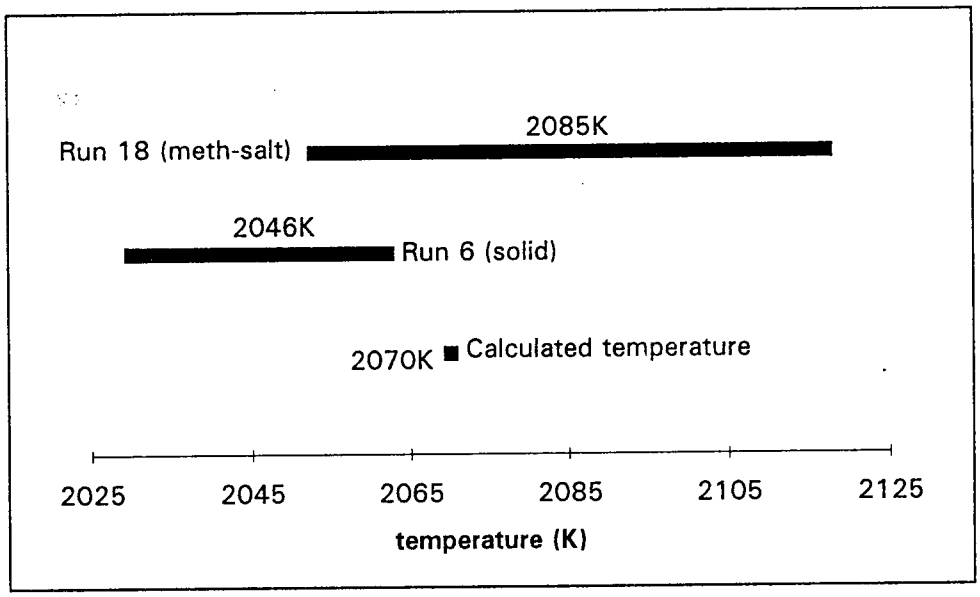


Fig. 6.7. Comparison of Calculated and Measured Temperatures

The expected temperature falls within the uncertainty values for Run 18. However, the Run 18 average temperature is higher than the calculated, and its helium arrival occurs before that of the calculated (from Fig. 6.3). This could suggest that the Mach number of Run 18 was slightly higher than 4.0. This would have indeed caused the temperature to be higher and the test duration time to be shorter. For comparison, the parameters for a shock of Mach 5.0 are calculated as being about 3000K for a duration of about 190μs [23].

The average temperature for Run 6 is lower than the calculated, possibly because the shock was less than Mach 4.0. This possibility is contradicted, however, by the observation that the duration of the higher temperature is 250μs, matching that taken from Fig. 6.3. A possible explanation could be due to the existence of the cool boundary layer in the shock tube. Solid sodium usage requires placing the salt on the bottom surface of the shock tube. It is expected that, when the shock front encounters the salt, some will remain in the boundary layer. Its presence will cause the measured temperature to be lower than it actually is because the sodium in the boundary layer will contribute to the measurement of the average temperature across the cross-section of the shock tube [11]. Therefore, a temperature correction due to the boundary layer must be applied. From Fig. 6.7, it is suggested that this correction is about 25K. In lieu of this correction, an additional uncertainty of -25K would be necessary. (In the comparison of the calculated value of temperature to those measured by the line reversal experiment, it must be noted that the uncertainty of the calculated value is unknown.)

Another observation that can be seen in Fig. 6.6 is the fact that the sodium does not begin emitting until about 30μs after the K6 trigger, also noted in Ref. [5]. If reactions near the shock front are of interest, the seeding method of using solid sodium would be a poor choice.

VII. Theoretical application to Impulse Facility

A. Description of Impulse Facility

The AEDC Impulse Facility is a reflected shock tunnel. It has a driver and driven section, much like the shock tube. Instead of having an intermediate chamber that is used to initiate the shock, as in the shock tube, the Impulse Facility uses a powder detonation to break the stainless steel diaphragm in its tube. The powder chamber is behind a piston. The detonation of the powder propels the piston into the driver gas, compressing it substantially, and increasing the pressure and temperature of the driver gas. This change causes the diaphragm to burst. The components making it a reflected shock tunnel are present near the test section. A diagram of this structure appears in Fig. 7.1 [25].

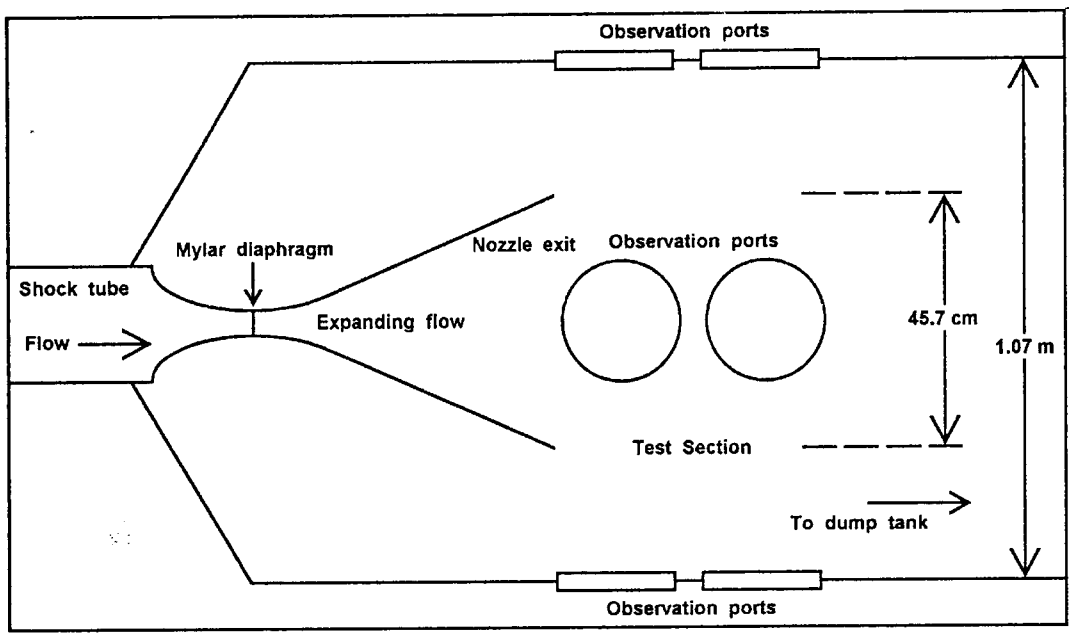


Figure 7.1. Diagram of Impulse Facility

The incident shock, coming down the shock tube after the rupture of the first diaphragm, arrives at the second diaphragm of 5mm thick Mylar, and is reflected from the converging nozzle inlet. This reflection causes reflected shock conditions of high pressure

and high temperature to develop in the plenum chamber to the left of the diaphragm before the incident shock bursts the second diaphragm. When the diaphragm has ruptured, the gas in the plenum chamber converges, reaching sonic speed at the throat, and then expands through the diverging exit nozzle. This expansion causes increasing velocity and decreasing temperature and pressure as the gas travels through the length of the nozzle [26]. Four sets of two observation ports are situated on the top, bottom, and sides of the test section. After passing these ports, the flow continues into a dump tank, or expansion chamber used to capture and slow the gas back down. It is followed by the cool, helium driver gas [27].

B. Optical arrangement

The SLR optical arrangement that would be used for the Impulse Facility is similar to that for the shock tube, except for two major differences. First, because of area limitations the cross axis configuration is not possible. Therefore, both beams would have to propagate in the same plane through the observation ports on the sides of the tunnel, but would cross in the middle to allow for viewing the same volume at the center of the tunnel. The second difference is a consequence of the size of the tunnel. For the flame and the shock tube, the distances involved were small enough that a focused optical system was possible. In the Impulse Facility, this is not the case. The light would be collimated before being directed through the test section, and then focused back down to be imaged onto the spectrometer slits. This constraint makes new optics necessary. The focal lengths of the lenses must be longer so that they can be placed at a distance of one focal length from the lamp filament, rather than two as for the focused system. The suggested arrangement is presented in Fig. 7.2.

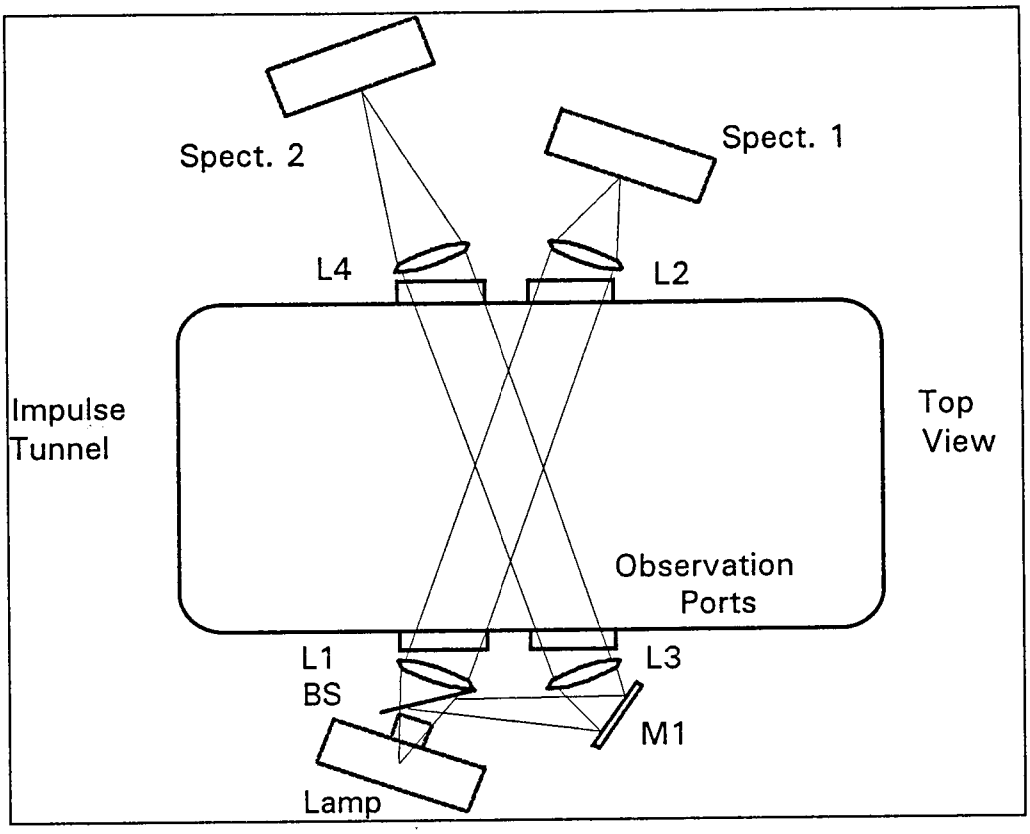


Figure 7.2. Experimental Set-up for Impulse Facility
View from the top

C. Introduction of sodium

The introduction of sodium would be by either a solution of methanol and salt or powdered solid salt. Both of these methods gave good results in the shock tube for different reasons. Weak signals occurred when the solution was used, but boundary layer effects in the shock tube seemed to have been negligible. Also, emission and absorption occurred almost immediately, albeit weakly. Runs with the powdered salt had strong signals in the shock tube relative to the noise, but boundary layer effects and delayed emission and absorption are drawbacks. For these reasons, each should be tried in the Impulse Facility.

The sodium seed would be placed in the exit nozzle. It would either be deposited in the nozzle on the downstream side of the Mylar diaphragm, or, more preferably, spread

onto the Mylar diaphragm, on the upstream side. The latter is preferred because, as reflected shock conditions are developing before breakage of the diaphragm, the sodium would be vaporizing so that lag times such as shown in Fig. 6.6 should not occur. With either method, though, it is thought that the sodium would be expanding and flowing with the test gas, thereby being carried rather uniformly into the test section.

For increased S/N ratio at the Impulse Facility, the PMTs should be cooled to decrease noise. Cooling units are available to accomplish this. With this addition, the low signal drawback of the methanol-salt solution may be avoided, and this method may be preferable over the powdered salt method.

D. Triggering, timing

Triggering at the Impulse Facility will be accomplished similarly to triggering in the shock tube. A detection gauge, ST6, corresponding to K5 in the shock tube, is located about 3in. upstream of the nozzle throat. This would be used to initiate the oscilloscope trace. The useful flow time of the Impulse Facility is estimated at about 3ms. Therefore, the total sweep time on the oscilloscope would be 5ms. It would allow for a pre-trigger of 0.5ms and have an ending time of 4.5ms after detection of ST6. This should allow for measurement of more than the entire flow, and a baseline noise level could be recorded in the time between ST6 and establishment of the flow.

E. Additional considerations

1. Doppler shifting

The optical set-up for the Impulse Facility requires passing the beams through the flow off of the axis perpendicular to the flow. Viewing in this manner will cause Doppler shifting of the spectral lines, and will actually appear as line broadening [7]. For an emitter approaching an observer with a velocity v_x, the Doppler shift is given by [7],

$$-\frac{\Delta\lambda}{\lambda_o}=\frac{v_x}{c}, \tag{15}$$

where $\Delta\lambda$ is the wavelength shift. This can be adapted to the optical arrangement at the Impulse Facility by knowing the viewing angle. For viewing at an angle θ to the flow, the Doppler shift is given by

$$-\frac{\Delta\lambda}{\lambda_o}=\frac{v_x\cos\theta}{c} \tag{16}$$

Given the dimensions of the observation ports in relation to each other, the observation angles may be calculated using trigonometry. With this in mind, the angles of observation would be 103.5^{o} and 76.5^{o}, where $\theta=0$ corresponds to the direction of v_X. For an average shock velocity, and the sodium wavelength of 589nm, these shifts would be $2.06\text{x}10^{-3}$nm and $-2.06\text{x}10^{-3}$nm, respectively. The resolution of the optical system limits the minimum $\Delta\lambda$ that can be observed for this wavelength range to about $1\text{x}10^{-2}$nm [28], almost an order of magnitude greater than the Doppler shifting. Therefore the shifting caused by off axis viewing will not introduce uncertainty.

2. Boundary layer

In the expansion nozzle of the Impulse Tunnel, there is a boundary layer of cool, slow moving gas. Also, at the exit of the nozzle, the gas exiting the nozzle is moving through gas that is at rest in the test section. This causes a shear layer from friction between the two gas masses. Because of the nozzle boundary and flow shear layers, there is difficulty in computational modeling and little information of the flow exiting the nozzle [29].

Pressure probe surveys have shown that there are no boundary layer effects in the center 12in. of the flow exiting the 18in. diameter nozzle, leaving 3in. on the outside circumference of the 18in. diameter nozzle in question [25].

The boundary layer is characterized by a decrease in temperature from its inner surface out. Once the temperature is less than approximately 1160K, the boiling point of sodium, no sodium emission or absorption occurs, and the cool portion of the boundary layer will not contribute to the measurement.

It would be beneficial to exclude sodium from the boundary layer. A suggested exclusion method would be to coat only a small, central fraction of the exposed Mylar diaphragm surface with the sodium seed, thereby keeping the seed away from the nozzle surfaces during the expansion. If this were the case, emission and absorption would only occur in the central region, where there are no boundary layer effects, as shown from probe data.

F. Expected results

As was previously mentioned, the expected duration of the useful Impulse Tunnel flow is 3ms. The expected temperatures, approximated using probe data, change according to the initial tunnel conditions. The uncertainties that the flow boundary layer could cause would result in a temperature reading that appeared too low, such as occurred in Run 6.

Optical transmission loss due to flow particulates can be a problem at the Impulse Facility; however, results could be corrected for any loss that occurred. Since the oscilloscope trace can be set to last longer than the flow, a measure of transmission loss may appear at the end of the trace. A better way, however, would be to correct the SLR data using transmission data acquired during every run of the tunnel. The deflection values of emission and absorption could be corrected for transmission percentage loss.

This would involve some uncertainty for the difference in oscilloscope sensitivity, and for the different wavelength of viewing. (The transmission measurement uses a helium-neon laser. Any correction involved would be small as this wavelength is relatively close to that of the sodium emission line.)

VIII. Conclusions and suggestions for future research

The sodium line reversal technique is very effective in measuring equilibrium temperatures between 1160K and 2600K. The lower bound is defined by the boiling point of sodium and the upper bound by the melting point of tungsten. Although the melting point of tungsten is actually about 3400K [13], it is recommended that the filament lamp be kept well below this temperature to prolong the life of the lamp.

During this work, successful measurements were made of the steady-state temperature of a flame and time resolved temperature of the flow in a shock tube. Several sodium introduction techniques were tried on both the flame and the shock tube with varying degrees of success. The measurements performed using the SLR technique compared favorably to other experimental temperature data , and also to calculated values for flames and shock tubes. Rigid uncertainty calculations showed that departures from these predicted temperatures that did occur were within the allowed uncertainty for the calibration of the optical system and the S/N of the electronic equipment. The culmination of these laboratory applications is a basis on which to propose application of this method to the Impulse Facility. The optical design, sodium introduction method, and triggering of electronic equipment have been outlined. Necessary additions to the SLR technique used in the flame and shock tube for adaptation to the Impulse Tunnel have been calculated and presented.

The SLR technique should be applied at the Impulse Facility. Temperature measurements using probes are intrusive and therefore not a preferred diagnostic method. Non-intrusive planar laser-induced fluorescence (PLIF) temperature measurements of nitric oxide have been performed at the Impulse Facility; however, only one instantaneous measurement can be made in the flow for each run. Also, helium arrival data, obtained as shown in Fig. 6.4, gives an overall arrival time, but SLR could provide validation of this measurement as seen in Figs. 6.5 and 6.6.

Prior to usage at the Impulse Facility, it is suggested SLR should be applied at the newly developed laboratory shock tunnel. This is a reflected shock tunnel scaled down from the size of the Impulse Tunnel to laboratory size. It is currently being used to replicate conditions in the Impulse Facility. Also, the use of two band filters, centered at the sodium line, should be considered to replace the spectrometers currently used in the experiment. These would allow more light to pass through them, therefore, a higher signal would be gathered at the PMTs than with the spectrometers in place.

In addition to this form of SLR being applied at the Impulse Facility, other optical techniques with wider temperature ranges should be applied. Replacement of the Tungsten strip lamp with a Xenon arc lamp having a color temperature of 6000K would provide a much higher temperature for use as a background source, although it would not be of variable temperature range as is the Tungsten lamp. Also, application of a pulsed electron gun is being investigated for temperature measurements at the Impulse Facility. It would allow for temperatures lower than those recognized by the line reversal method to be measured. Also, the high intensity of the beam would eliminate optical transmission problems that are sometimes a concern in the Impulse Tunnel.

References

References

1. Gaydon, A.G. and Wolfhard, H.G., Flames: Their Structure, Radiation and Temperature, John Wiley & Sons, New York, 1979.

2. Cattolica, Robert J., Combustion Sciences Department, Sandia National Laboratories, "OH Radical Nonequilibrium in Methane-Air Flat Flames", Combustion and Flame 44: 43-59 (1982).

3. Winkleman, Bradley Carl, Gas Temperature Measurements of Fluctuating Coal Fired MHD Plasmas Using Modified Line Reversal, Doctoral Dissertation, UTSI, August, 1992.

4. Bauman, Leslie E., et. al., "Measurements of Temperature and Seed Atom Density in High-Speed MHD Flows", Journal of Thermophysical and Heat Transfer, Vol. 8, No. 3, July-September, 1994.

5. Clouston, J.G., Gaydon, A.G., F.R.S., and Hurle, I.R., "Temperature Measurements of Shock Waves by Spectrum-Line Reversal", Proceedings Roy. Soc. A, Vol. 252, pp.429-444.

6. Clouston, J.G., Gaydon, A.G., F.R.S., and Hurle, I.R., "Temperature Measurements of Shock Waves by Spectrum-Line Reversal (A Double-Beam Method)", 26 March 1959, Proceedings Roy. Soc. A, Vol. 252, pp. 143-155.

7. Thorne, Anne P., Spectrophysics, J. W. Arrowsmith Ltd, Bristol, 1988.

8. Griem, Hans R., Plasma Spectroscopy, McGraw Hill Book Company, New York, 1964

9. DeVos, J.C., "A New Determination of the Emissivity of Tungsten Ribbon", Physica, 20, Oct. 1954, pp. 690-715.

10. Larrabee, Robert D., "Spectral Emissivity of Tungsten", July 7, 1958, Journal of the Optical Society of America, vol. 49, no. 6, pp. 619-625.

11. Gaydon, A.G. and Hurle, I.R., The Shock Tube in High-Temperature Chemical Physics, Reinhold Publishing Corporation, New York, 1963

12. Greig, J.R., The Sodium D-Line Reversal Method of Temperature Measurement in Ionized Flame Gases, Brit. J. Applied Physics, Vol. 16, 1965.

13. Lide, David R., CRC Handbook of Chemistry and Physics: 71st edition, CRC Press, Inc., 1990.

14. Mak, W.H., "Sodium Line Reversal Temperature Measurements in Shock Tube Flows", UTIA Technical Note No. 66, 1963.

15. Herzberg, G., Atomic Spectra and Atomic Structure, Dover Publications, New York, 1944.

16. Williams, W.D., Private Communication.

17. Baird, D.C., Experimentation: An Introduction to Measurement Theory and Experimental Design, Prentice Hall, Inc., Englewood Cliffs, New Jersey, 1962.

18. McKenna Products, Inc., Flat Flame Burner Specifications and Product List, Pittsburg, California, January 15, 1993.

19. Michalski, L. et. al., Temperature Measurement, John Wiley and Sons, Chichester, 1991.

20. Incropera, Frank P.; De Witt, David P., Fundamentals of Heat and Mass Transfer (third edition), John Wiley and Sons, New York, 1990.

21. Pruitt, David, Sverdrup/AEDC, NASA SP-273 Chemical Equilibrium Program operation.

22. Smith, M.S., Williams, W.D., Price, L.L., Jones, J.H., "Shocktube Planar Laser Induced Fluorescence Measurements in Support of the AEDC Impulse Facility", 18th AIAA Aerospace Ground Testing Conference, June 20-23, 1994, Colorado Springs, CO.

23. Smith, Michael S., Processes Occurring in a Pressure-Driven Shock Tube, Master's Thesis, UTSI, August, 1984.

24. AEDC Fact Sheet, "Results of Diagnostic Measurements in Impulse Shock Tunnel", Office of Public Affairs, Arnold Engineering Development Center, 1995.

25. Blanks, J.R:, DeWitt, J.R., "Calibration Tests of AEDC Free-Piston Shock Tunnel", 18th AIAA Aerospace Ground Testing Conference, June 20-23, 1994, Colorado Springs, CO.

26. Anderson, John David, Hypersonic and High Temperature Gas Dynamics, McGraw-Hill, Inc., 1989.

27. Byun, Y.; Lee, J.Y.; Anderson, Jr., J.D.; Kothari, A.P., "Unsteady Hypersonic Viscous Flow in Impulse Facilities", 28th AIAA Aerospace Sciences Meeting, January 8-11, 1990.

28. Sears, Francis Weston, Optics, Addison-Wesley Publishing Company, Inc., Cambridge, Mass, 1956.

29. Maus, Jim, Private Communication.

30. McQuarrie, Donald A., Statistical Mechanics, Harper & Row Publishers, Inc, New York, NY, 1976.

Appendices

Appendices

A. SODREV3.FOR

```
      PROGRAM SODREV
C     4/8/94
C     Program to compute the temperature of shock heated gas by use
C     of a double beam method for Na line reversal.  Used in calculation
C     for the flat flame burner.
C
C     Defined variables:
C           c1: first radiation constant (Watts*meters**2/ster)
C           c2: second radiation constant (meters*degrees Kelvin)
C           t: trans. coefficient of the lamp window (quartz)
C           tl: trans. coef. of focusing lens
C           tw: trans. coef. of shock tube window
C           rm1: reflectance coef. of mirror 1 for beam 2
C           rm2: Ref. coef. of mirror 2 for beam 2
C           rbeam: Ref. coef. of beamsplitter
C           tbeam: trans. coef. of beamsplitter
C           wave: wavelength of interest (meters) 589 E-9
C
C     Input variables:
C           tb: brightness temp. calculated using spec. rad. calibration
C
C     Calculated variables:
C           tmax: high temperature for emissivity iteration
C           tmin: low temperature for emissivity iteration
C           tt: true temperature of the lamp
C           t1: temp. of beam one with losses accounted for
C           t2: temp. of beam two with induced losses accounted for
C           E(): emis. of tungsten at () temp. and 589 nm
C           tg: actual temperature of the gas.

      CHARACTER*8  FILEN
      DIMENSION  FE(20), E(8), TEMP(8)
      DATA TEMP/1000.0, 1200.0, 1400.0, 1600.0, 1800.0, 2000.0,
     * 2200.0, 2400.0/
      DATA E/0.4642, 0.4600, 0.4568, 0.4529, 0.4493, 0.4456,
     * 0.4422, 0.4392/

      WRITE(*,*) 'FILENAME FOR OUTPUT?'
      READ(*,95) FILEN
95    FORMAT(A8)
```

```
      OPEN (UNIT=20, FILE=FILEN, STATUS='NEW')

      C1=1.191062E-16
      C2=0.01438786
      WAVE=589.0E-9
      T=0.93
      TL=0.93
      TW=1.0
      RM1=0.92
      RM2=0.99
      RBEAM=.20
      TBEAM=.55

      WRITE (*,*) 'Tb(include 1 decimal place)?'
      READ (*, 15) TB
15    FORMAT (F7.1)


C     This calculation finds the temperature and emissivity bounds for
C     the beam temperature calculations.
        ATT = 1.0/TB + (WAVE/C2) * LOG(0.45*T)
        TT  = 1.0/ATT

        DO 29 L=1, 8
       IF ((TEMP(L)-TT).LE.200.AND.(TEMP(L)-TT).GE.0) THEN
            TMAX = TEMP(L)
            ETMAX = E(L)
          END IF
          IF ((TTTEMP(L)).LE.200.AND.(TTTEMP(L)).GE.0) THEN
            TMIN = TEMP(L)
            ETMIN = E(L)
          END IF
29      CONTINUE
        WRITE(20,75) 'TMAX', 'ETMAX', 'TMIN', 'ETMIN'
75      FORMAT(/A10,A8,A10,A8)
        WRITE(20,25) TMAX,ETMAX,TMIN,ETMIN
25      FORMAT (F10.1, F8.4, F10.1, F8.4/)

        WRITE(20, 85) 'TB =', TB, 'EMIS', 'Tt', 'T1', 'T2'

85      FORMAT (1X,A5,F7.1,/3X,A4,12X,A2,14X,A2,14X,A2,/ 60('='))

C     This iterative calculation calculates the true temperature and
C     the beam temperatures from the input brightness temperature.
        DO 9 I = 1, 10
```

```
      FE(I) = ETMAX + (ETMIN - ETMAX)*((TMAX-TT)/(TMAX-TMIN))
          ATT = 1.0/TB + (WAVE/C2) * LOG(FE(I)*T)
          TT  = 1.0/ATT
C     Calculation to find the beam one temperature from the calculated
C     value of tt.
          AT1 = 1.0/TT - (WAVE/C2) * LOG(T*TBEAM*TL*TW)
          T1 = 1.0/AT1
C     Calculation to find the beam two temperature from the calculated
C     value of tt.
        AT2 =1.0/TT - (WAVE/C2) * LOG(T*RBEAM*RM1*TL*RM2*TW)
          T2 = 1.0/AT2
          WRITE(20, 35) FE(I), TT, T1, T2
35      FORMAT (1X, F7.5, 6X, F10.1, 6X, F10.1, 6X, F10.1)
9       CONTINUE

        WRITE(*, 85) 'TB =', TB, 'EMIS', 'Tt', 'T1', 'T2'
        WRITE(*, 105) FE(10), TT, T1, T2
105     FORMAT (1X, F7.5, 6X, F10.1, 6X, F10.1, 6X, F10.1/)

C     Now need to take in deflection values for the two PMTs to
C     calculate the actual temperature of the gas.

        WRITE (*,*) 'For a deflection in the wrong direction, enter as a
     *negative value.'
        WRITE (*,*) 'PMT1 deflection into absorption?'
        READ (*,45) A
        WRITE (*,*) 'PMT2 deflection into emission?'
        READ (*,45) B
45      FORMAT (F5.3)
        TG = (A*T2 + B*T1)/(A+B)
C     For a deflection in the wrong direction, enter as a negative value.
        WRITE (*,55) 'TG =', TG
        WRITE (20, 55) 'TG =', TG
55      FORMAT (/, A5, F7.1)

C     105, 29

        END
```

B. SODREV4.FOR

```
      PROGRAM SODREV
C     2/14/95
C     Program to compute the temperature of shock heated gas by use
C     of a double beam method for Na line reversal.  Used in calculation
C     for the shock tube, where a temperature curve in time is necessary.
C     Defined variables:
C           c1: first radiation constant (Watts*meters**2/ster)
C           c2: second radiation constant (meters*degrees Kelvin)
C           t: trans. coefficient of the lamp window (quartz)
C           tl: trans. coef. of focusing lens
C           tw1: trans. coef. of shock tube window in beam 1
C           tw1: trans. coef. of shock tube window in beam 2
C           rm1: reflectance coef. of mirror 1 for beam 2
C           rm2: Ref. coef. of mirror 2 for beam 2
C           rbeam: Ref. coef. of beamsplitter
C           tbeam: trans. coef. of beamsplitter
C           wave: wavelength of interest (meters) 589 E-9
C
C     Input variables:
C           tb: brightness temp. calculated using spec. rad. calibration
C           A: PMT1 deflection into absorbsion
C           B: PMT2 deflection into emission
C
C     Calculated variables:
C           tmax: high temperature for emissivity iteration
C           tmin: low temperature for emissivity iteration
C           tt: true temperature of the lamp
C           t1: temp. of beam one with losses accounted for
C           t2: temp. of beam two with induced losses accounted for
C           E(): emis. of tungsten at () temp. and 589 nm
C           tg: actual temperature of the gas.

      CHARACTER*8  FILEN, FILEN1
      DIMENSION  FE(20), E(8), TEMP(8), A(125), B(125), Tg(125)
      DATA TEMP/1000.0, 1200.0, 1400.0, 1600.0, 1800.0, 2000.0,
     * 2200.0, 2400.0/
      DATA E/0.4642, 0.4600, 0.4568, 0.4529, 0.4493, 0.4456,
     * 0.4422, 0.4392/

      WRITE(*,*) 'FILENAME FOR OUTPUT?'
      READ(*,95) FILEN
95    FORMAT(A8)
```

```
      OPEN (UNIT=20, FILE=FILEN, STATUS='NEW')

      C1=1.191062E-16
      C2=0.01438786
      WAVE=589.0E-9
      T=0.93
      TL=0.93
      TW1=0.91
      TW2=0.94
      RM1=0.92
      RM2=0.92
      RBEAM=.20
      TBEAM=.55

      WRITE (*,*) 'Tb(include 1 decimal place)?'
      READ (*, 15) TB
15    FORMAT (F7.1)

      WRITE (*,*) 'FILENAME FOR DEFLECTION INPUT?'
      READ (*,125) FILEN1
125   FORMAT (A8)
      OPEN (UNIT=30, FILE=FILEN1, STATUS='OLD')

C     This calculation finds the temperature and emissivity bounds for
C     the beam temperature calculations.
      ATT = 1.0/TB + (WAVE/C2) * LOG(0.45*T)
      TT  = 1.0/ATT

      DO 29 L=1, 8
      IF ((TEMP(L)-TT).LE.200.AND.(TEMP(L)-TT).GE.0) THEN
          TMAX = TEMP(L)
          ETMAX = E(L)
        END IF
        IF ((TT-TEMP(L)).LE.200.AND.(TTTEMP(L)).GE.0) THEN
          TMIN = TEMP(L)
          ETMIN = E(L)
        END IF
29    CONTINUE
      WRITE(20,75) 'TMAX', 'ETMAX', 'TMIN', 'ETMIN'
75    FORMAT(/A10,A8,A10,A8)
      WRITE(20,25) TMAX,ETMAX,TMIN,ETMIN
25    FORMAT (F10.1, F8.4, F10.1, F8.4/)

      WRITE(20, 85) 'TB =', TB, 'EMIS', 'Tt', 'T1', 'T2'
```

```
85        FORMAT (1X,A5,F7.1,/3X,A4,12X,A2,14X,A2,14X,A2,/ 60('='))

C       This iterative calculation calculates the true temperature and
C       the beam temperatures from the input brightness temperature.
          DO 9 I = 1, 10
         FE(I) = ETMAX + (ETMIN - ETMAX)*((TMAX-TT)/(TMAX-TMIN))
            ATT = 1.0/TB + (WAVE/C2) * LOG(FE(I)*T)
            TT  = 1.0/ATT
C       Calculation to find the beam one temperature from the calculated
C       value of tt.
            AT1 = 1.0/TT - (WAVE/C2) * LOG(T*TBEAM*TL*TW1)
            T1 = 1.0/AT1
C       Calculation to find the beam two temperature from the calculated
C       value of tt.
          AT2 =1.0/TT - (WAVE/C2) * LOG(T*RBEAM*RM1*TL*RM2*TW2)
            T2 = 1.0/AT2
            WRITE(20, 35) FE(I), TT, T1, T2
35        FORMAT (1X, F7.5, 6X, F10.1, 6X, F10.1, 6X, F10.1)
9         CONTINUE

          WRITE(*, 85) 'TB =', TB, 'EMIS', 'Tt', 'T1', 'T2'
          WRITE(*, 105) FE(10), TT, T1, T2
105       FORMAT (1X, F7.5, 6X, F10.1, 6X, F10.1, 6X, F10.1/)

C       Now need to take in deflection values for the two PMTs to
C       calculate the actual temperature of the gas.

C       For a deflection in the wrong direction, enter as a negative value.

          WRITE (20,155) ' Chan 1', ' Chan 2', '  Temp.'
155       FORMAT (/1X, A8, A16, A16/)
          J=1
39        CONTINUE
            READ (30,135, END=49) A(J), B(J)
135         FORMAT (F9.6, F16.6)
            Tg(J) = (A(J)*T2 + B(J)*T1)/(A(J)+B(J))
            WRITE (20,145) A(J), ',', B(J), ',', Tg(J)
145         FORMAT (1X, F8.6, A2, F8.6, A2, F8.1)
            J=J+1
          GO TO 39
49        CONTINUE

C       155, 49

          END
```

Vita

Kathleen Patricia Baker was born in Youngsville, NY on March 5, 1971. She attended Jeffersonville-Youngsville Central School in Jeffersonville, NY and graduated in 1989, third in her class. Following this, in 1989 she enrolled at the University of Scranton, Scranton, PA to pursue a Bachelors degree. While there she was listed in "Who's Who Among Students in American Colleges and Universities". In 1993, she graduated, receiving a Bachelor of Science degree in Physics.

In the fall of 1993, she accepted a graduate research assistantship at the University of Tennessee Space Institute. She was placed at Arnold Engineering Development Center, Arnold Air Force Base, TN, with the Hypersonics Flow Diagnostics group of Calspan Corporation, later to be known as Micro Craft Technology. She was awarded the Master of Science degree in Physics in August of 1995.